External mechanical cues reveal core molecular pathway behind tissue bending in plants

Authors: Anirban Baral[1,*], Emily Morris[2,b], Bibek Aryal[1,3], Kristoffer Jonsson[1], Stéphane Verger[1], Tongda Xu[4], Malcolm Bennett[2], Olivier Hamant[5], Rishikesh P. Bhalerao[1,*,†]

Affiliations:

[1]Umeå Plant Science Centre, Department of Forest Genetics and Plant Physiology, Swedish University of Agricultural Sciences, 901 87 Umeå, Sweden,

[2]Centre for Plant Integrative Biology, University of Nottingham, Nottingham LE12 SRD, UK,

[3]Beijing Advanced Innovation Center for Tree Breeding by Molecular Design, Beijing Forestry University, Beijing 100083, China,

[4]FAFU-Joint Centre, Horticulture and Metabolic Biology Centre, Haixia Institute of Science and Technology, Fujian Agriculture and Forestry University, Fuzhou, Fujian 350002, China,

[5]Laboratoire de Reproduction et Développement des Plantes, Université de Lyon, ENS de Lyon, UCBL, INRA, CNRS, 46 Allée d'Italie, 69364, Lyon, Cedex 07, France,

[b]Current address: Oxford University Innovation, Buxton Court, 3 West Way, Oxford OX20JB, UK.

[†]Lead contact: Rishikesh P Bhalerao.

*For correspondence: abaral1986@gmail.com (A.B); Rishi.Bhalerao@slu.se (R.P.B)

Summary

Tissue folding is a central building block of plant and animal morphogenesis. In dicotyledonous plants, hypocotyl folds to form hook after seedling germination that protects their aerial stem cell niche during emergence from soil. Auxin response factors and auxin transport are classically thought to play a key role in this process. Here we show that the microtubule-severing enzyme katanin contributes to hook formation. However, by exposing hypocotyls to external mechanical cues mimicking the natural soil environment, we reveal that auxin response factors ARF7/ARF19, auxin influx carriers, and katanin are dispensable for apical hook formation, indicating that these factors primarily play the role of catalyzers of tissue bending in the absence of external mechanical cues. Instead, our results reveal the key roles of the non-canonical TMK-mediated auxin pathway, PIN efflux carriers and cellulose microfibrils as components of the core pathway behind hook formation in presence or absence of external mechanical cues.

Keywords

Tissue folding, Differential growth, mechanical cues, microtubule, cellulose, auxin.

Introduction

Tissue folding is an essential feature of body plan development across kingdoms. In animals, tissue rearrangements can generate patterns of tension and compression, which in turn contribute to tissue invagination during gastrulation, through the actomyosin mediated response to forces [1-3]. Interestingly, such intrinsic mechanical cues can be artificially mimicked by external mechanical cues in the form of local indentations; even rescuing tissue invagination defects in *Drosophila* myosin mutants [4]. This calls for an investigation of the relative contribution of intrinsic and external mechanical cues to development. In animals the core developmental plan is laid out in the embryo stage, and since animal embryos are usually embedded in a protective shell, such external cues are likely to be filtered out. In contrast, the postembryonic development of plants are constantly exposed to both internal and external mechanical constraints Here we investigate how plants cope with such conflicting cues to control tissue folding.

The presence of stiff cell walls and high turgor pressure in plants limit certain mechanisms of differential growth such as cell migration and cell contraction. However, because plant cells are tightly attached to one another through their contiguous walls, local differences in cell elongation is employed to create pronounced deformations in tissue and organ shape [5]. In keeping with their sessile lifestyle, land plants have also acquired the unique ability to substantially alter their shape and form to adapt to their environment. The genetic and biochemical pathways that regulate differential growth in plants**,** and their modulation by exogenous cues**,** have been investigated in numerous studies; reviewed in [6]. In addition to biochemical signals, a critical role for mechanical signals in regulating plant development is emerging. Touch or wind has a genome-wide impact on the transcriptome, leading to wall stiffening and reduced stature [7] Mechanical signals can also arise internally: turgor pressure puts walls and tissues under tension [8], and mechanical conflicts arise between cells and tissues with different growth parameters, as seen in shoot apical meristems [9], sepals [10] and leaves [11].

Hypocotyl bending to form an (apical) hook is facilitated by differential cell elongation. Polar transport-mediated accumulation of auxin on one side of the hypocotyl restricts the elongation of epidermal cells [12], forming the concave side of the apical hook. Such tissue folding reflects a mechanical conflict across the structure [13]. Interestingly, the

apical hook forms during germination in the absence of external constraints in petri dishes, while under native growth conditions, hook development proceeds under mechanical constraints imposed by the soil [12]. We are using tissue bending in the hypocotyl during seed germination as an experimental model to study how exposure to exogenous cues from mechanical constraints during soil emergence as well as endogenous cues can modulate shape change through differential growth and tissue folding.

In plants, cortical microtubules (CMTs) are key players in morphogenesis; they mediate the deposition of cellulose microfibrils and confer directionality during cell elongation. Interestingly, CMTs have been shown to align with directions of maximal tensile stress that tissue shape and/ or growth imposes [9, 14, 15]. However, exogenously applied force can override the endogenous stress pattern and reorient CMTs [9, 16]. The protein katanin plays a key role in promoting CMT self-organization in response to such cues, by severing nascent microtubule branches and microtubule crossovers as well as promoting microtubule bundling [17]. In loss-of-function katanin mutants, CMT arrays are slow to self-organize in parallel bundles and thus usually appear disorganized [18]. CMTs in these mutants react slowly to both endogenous and exogenous mechanical cues [9, 10, 15]. However, attaining anisotropic CMT orientation even in the absence of katanin activity is theoretically possible through growth, cell shape and geometry-induced self-organization of CMTs [19] and from directional stabilization of CMT arrays by prolonged exogenous mechanical cues [14]. It seems therefore that exogenous and endogenous mechanical stress can act in synergy to control CMT organization. However, the significance of this balance of growth processes remains to be demonstrated.

Through the study of hypocotyl bending during hook formation under mechanical constraints imposed by soil**,** we identified a role for dynamic rearrangement of CMTs in tissue folding, in response to both internal and external mechanical cues. Importantly**,** our results demonstrate that external mechanical constraints can rescue tissue folding defects in the katanin mutants. The associated mechanism is dependent on cellulose microfibril organization and on the polar auxin transport machinery, and it requires an alternative auxin response pathway mediated via the TMK receptor kinase to facilitate tissue bending and apical hook formation.

Results:

Apical hook formation depends on katanin-dependent microtubule organization

To assess the mechanisms underlying tissue bending under mechanical constraints we used apical hook development as a model. Since CMTs are key morphogenetic regulators, we first assessed their role in hypocotyl bending and hook development. We compared hook formation in WT and the *ktn1-5* mutant [20] which lacks the microtubule-severing enzyme katanin. Whereas WT seedlings formed closed apical hooks approximately 30 Hrs after germination (Figure 1A, left), *ktn1-5* mutant seedlings could not achieve hypocotyl bending and their hooks were open (Figure 1A, right). Using time-lapse infrared imaging [21] we observed that *in vitro*-grown WT seedlings formed closed apical hooks by progressive bending the hypocotyl within 24-26 Hrs of germination**.** After 28 Hrs, hooks of all the WT seedlings were closed (hook angle of 180°) (Figure. 1B). In contrast, *ktn1-5* seedlings growing on the agar surface were unable to form this bend and 28 Hrs after germination their hook angles were much smaller (53.89 ± 25.63°, n = 20), (Figure. 1B)

CMT organization has been associated with stem curvature in response to gravistimulation or forced bending [22]. Here we characterized CMT arrangement in WT hooks compared to *ktn1-5.* We used the reporter microtubule-associated protein 4 fused with green fluorescent protein (GFP-MAP4) to visualize microtubules [23] and the FibrilTool plugin [24] to quantify CMT arrangement (array anisotropy) across the hypocotyl. In WT hooks CMT arrays were significantly more anisotropic (anisotropy value 0.27 ± 0.009 SEM, n = 250 cells) on the convex side of the hook than on the concave side (anisotropy value 0.18 ± 0.001 SEM, n = 251 cells) (Figure. 1C, 1D). In contrast, CMT arrays in *ktn1-5* showed significant reduction in anisotropy and there was little difference in array anisotropy across the two sides of the hypocotyl (Figure. 1E, 1F, side1 *vs* side2; anisotropy values 0.084 ± 0.003 SEM, n = 221 cells and 0.085 ± 0.002 SEM, n = 179 cells). These results suggest that the difference in CMT organization on the two sides of the hypocotyl is associated with tissue bending during hook development and its disruption is associated with defects in hook formation.

134

135 **Apical hook defect in a *katanin mutant* can be rescued by external constraints**

136 Typically, upon germination, emerging seedlings are exposed to physical, biochemical
137 and biological constraints by the soil. Hence we investigated the role of microtubules in
138 hook formation in wild type and *ktn1-5* under natural conditions by germinating seeds
139 within sterile soil and imaging hook formation using non-invasive X-ray microcomputed
140 tomography [25]. Intriguingly, hypocotyl bending and formation of closed hooks were
141 observed in *ktn1-5* seedlings growing through the soil (Figure. 1G). Thus, despite the
142 inability to form a hook on the agar surface, during growth in soil (a more natural condition
143 for germinating seeds), the *ktn1-5* hypocotyl was able to bend and form a hook.
144 To focus on the physical contribution of the soil to this response, we investigated hook
145 formation by germinating seeds inside agar (as a proxy for soil). Using time-lapse infrared
146 imaging [21], we observed that hooks of all the WT seedlings were closed (hook angle of
147 180^0) both on the surface and in agar. Hook angles of constrained (agar-grown) and free
148 (surface-grown) WT seedlings were similar, suggesting that mechanical constraints do
149 not amplify hook bending (Figure. 1B). Intriguingly, germination in agar significantly
150 alleviated hook defects in *ktn1-5* seedlings and after 28 Hrs post-germination their hook
151 angles were much larger (162.06 ± 17.8°, n= 20), when compared to surface-grown *ktn1-*
152 *5* seedlings, i.e. those not exposed to external mechanical constraints (Figure. 1B).

153 ***katanin* rescue by external constraints relies on microtubule dynamics**

154 The developmental defects seen in the *ktn1-5* mutant are attributed to the CMT
155 disorganization associated with loss of the microtubule-severing and bundling activities
156 of katanin [17]. In the most parsimonious scenario, reestablishment of apical hook
157 formation by mechanical cues in *ktn1-5* could suggest that microtubules are not essential
158 for bending in response to mechanical cues during growth in soil. To check this
159 hypothesis, we used pharmacological and genetic approaches. Treatment with low
160 concentrations of the microtubule-depolymerizing drug oryzalin (200 nM) or the
161 microtubule-stabilizing drug paclitaxel (50 nM), which did not affect WT seedlings (Figure.
162 S1A, S1C), completely abolished hook formation in *ktn1-5* seedlings grown in agar
163 (Figure. S1B, S1D). Additionally, genetically perturbing CMT rearrangement by

164 introducing the *tua5*^{D251N} mutation (which slows down microtubule dynamics) [26] in *ktn1-*
165 *5* also abolished hook formation in response to mechanical constraints (Figure. S1F).
166 Thus, even in the absence of katanin, microtubule dynamics is required for apical hook
167 formation.
168 When mechanical stress levels are increased in the shoot apical meristem (e.g. upon wall
169 weakening with the cellulose synthase inhibitor isoxaben), CMTs can exhibit WT-like
170 behavior in a *katanin* mutant, where they can reorient around a single cell ablation as in
171 WT [9]. We reasoned that soil, or agar gel, may provide a mechanical cue strong enough
172 to compensate for the slower CMT dynamics in the *katanin* mutant. To test this
173 hypothesis, we investigated whether constrained growth in agar could facilitate a
174 difference in CMT organization in the *ktn1-5* mutant. In contrast to the lack of significant
175 difference in CMT array anisotropy in surface-grown *ktn1-5* seedlings, growth under
176 mechanical constraints resulted in a significant difference in CMT array anisotropy
177 between the two sides of *ktn1-5* mutant hypocotyls (Figure. 1H, 1I; anisotropy value of
178 0.15 ± 0.003 SEM, n = 315 cells on convex side *vs* 0.09 ± 0.002 SEM, n = 360 cells on
179 concave side). Note that absolute anisotropy values were lower in *ktn1-5* than in the WT,
180 suggesting that the relative difference in CMT behavior between the two sides of the
181 hypocotyl may be sufficient for tissue bending. Taken together our results indicate that
182 external mechanical cues can catalyze the formation of differential CMT organization on
183 both sides of the hypocotyl to induce tissue bending.

184 **Cellulose microfibril deposition is critical for mechanically-induced hook formation**

185 From the close association of CMTs and cellulose synthase complexes [27] it can be
186 surmised that CMTs would guide the deposition of cellulose microfibrils to promote hook
187 formation. To formally check this, we first examined hook formation in two mutants with
188 altered cellulose content and cellulose organization: the cellulose synthase A1 (CesA1)
189 mutant *any1***,** with reduced crystalline cellulose content [28]**,** and the cellulose synthase
190 interacting 1 (CSI1) protein deficient mutant *pom2-8* [29]**,** featuring altered cellulose fiber
191 orientation arising from the partial decoupling of CesA complex from CMTs. As expected,
192 both *any1* and *pom2-8* mutants had defects in hook formation (Figure 2A, 2B). However,
193 unlike *ktn1-5,* hook formation in *any1* and *pom2-8* mutants was not appreciably

194 suppressed by growth inside agar (Figure. 2A, 2B). These results further suggest that the
195 rescue of the *ktn1-5* hook defect by growth in agar requires CMT-guided cellulose
196 deposition. To test this, we introduced *any1* and *pom2-8* mutations into the *ktn1-5*
197 background. Hook formation could not be restored in agar-grown *ktn1-5 any1* or *ktn1-5*
198 *pom2-8* double mutant seedlings (Figure. 2C, 2D). We also found that hook formation in
199 agar-grown *ktn1-5* seedlings was hypersensitive (Figure. S2) to 100 nM 2,6-
200 dichlorobenzonitrile (DCB), a cellulose biosynthesis inhibitor [30]. Hence, both genetic
201 and pharmacological approaches demonstrate the crucial role of cellulose organization
202 in mediating the bending required for hook formation in response to mechanical cues.

203 **Differential growth mediated by mechanical cues is dependent on auxin response**
204 **asymmetry**

205 Hypocotyl bending during apical hook formation results primarily from differences in
206 epidermal cell elongation between the sides [31]. Consistent with this, and because there
207 is limited cell division at this stage [32], epidermal cell length was significantly different
208 between the concave (34.26 ± 0.11 μm SEM, n = 250 cells) and convex (61.39 ± 2.86 μm
209 SEM, n = 251 cells) sides of the WT hook (Figure 3A). In sharp contrast, epidermal cell
210 lengths in *ktn1-5* were similar on both sides of the hypocotyl (Figure. 3B, side 1 vs side
211 2); cell length 53.85 ± 1.592 μm SEM, n = 221 cells and 61.90 ± 2.02 μm SEM, n = 179
212 cells. As expected, when grown inside agar, cell length difference across the hypocotyl
213 was re-established in *ktn1-5* seedlings (Figure. 3C); cell length of 33.02 ± 0.64 μm SEM,
214 n = 360 cells on the concave side *vs* 63.24 ± 1.2 μm SEM, n = 351cells on the convex
215 side. The cells on the concave (inner) side of mechanically constrained *ktn1-5* seedlings
216 were significantly smaller than cells on either side of surface-grown *ktn1-5* seedlings
217 (Figure. 3D). These results suggest that growth asymmetry mediated by repression of
218 growth on one side can be reestablished in *ktn1-5* seedlings grown under mechanical
219 constraint.
220 The repression and slower rate of cell elongation can be attributed to auxin response
221 maxima forming on the concave side [33]. Mechanical constraints in agar-grown
222 hypocotyls could simply deform the hypocotyl resulting in bending through a direct impact
223 on CMTs. Alternatively, mechanical cues may influence the auxin response, modifying

224 differential growth, and indirectly affecting CMTs. To address this, we first investigated
225 whether impaired hook formation in *ktn1-5* seedlings is due to attenuation of the auxin
226 response. In WT hooks, auxin response maxima, visualized using the synthetic auxin
227 reporter DR5:: Venus-N7 [34], were seen only on the concave side (Figure. 3E, left):
228 whereas the *ktn1-5* seedlings failed to establish this asymmetry; DR5:: Venus-N7 signals
229 were seen on both sides of the hypocotyl (Figure. 3E, middle). We then investigated
230 whether constrained growth in agar gel could reestablish DR5:: Venus-N7 signal
231 asymmetry in a katanin-independent manner. In *ktn1-5* seedlings grown inside agar, the
232 DR5:: Venus-N7 signal was observed only on the concave side (Figure. 3E, right). Lastly,
233 microtubule perturbation with 200 nM oryzalin abolished establishment of DR5:: Venus-
234 N7 signal asymmetry in *ktn1-5* seedlings grown inside agar (Figure. S3B). These data
235 suggest that mechanical constraints in agar-grown hypocotyls induce hook formation by
236 establishing auxin response asymmetry, and the resulting mechanical conflict would be
237 strong enough to override reduced CMT dynamics in the *katanin* mutant.
238

239 **Mechanical constraints can modulate polar auxin transport during apical hook**
240 **formation**

241 To decipher the link between external mechanical constraints and differential auxin
242 response in the apical hook, we next analyzed the contribution of auxin transporters.
243 Auxin influx carriers of the AUX/ LAX family are thought to play an important role in auxin
244 response asymmetry in the apical hook [35]. Consistently, hook formation was severely
245 affected in the *aux1 lax1 lax2 lax3* quadruple mutant when grown on the surface,
246 mimicking the *ktn1*-5 mutant phenotype (Figure. S4A). As observed for *ktn1-5*, growth
247 inside agar could restore hook formation in this *aux/ lax* quadruple mutant (Figure. S4A),
248 as observed for *ktn1-5*. Thus hook formation does not require AUX/LAX auxin influx
249 carriers.
250 The efflux carriers of the PIN-FORMED (PIN) family are also thought to be required for
251 hook formation [33]. Similar to AUX/ LAX carriers, hook formation was also completely
252 abolished in the *pin1347* quadruple mutant when grown on the surface (Figure. S4B).
253 However, in contrast with *aux/ lax* or *ktn1-5* mutants, hook formation did not occur in
254 *pin1347* (Figure. S4B) even when grown inside agar. Thus external mechanical cues can

255 override both katanin-dependent CMT dynamics and AUX/ LAX-dependent auxin influx,
256 but they require PIN auxin transporters for hook formation.
257 Tissue- and cell-type-specific polar localization of PIN transporters is critical for the
258 directional flow of auxin [36]. For the PINs implicated in hook development (PIN1, 3, 4
259 and 7), PIN4-GFP signal could be detected only in the epidermal cells. The localization
260 of PIN4-GFP was strongly polar with preferential localization to transverse membranes
261 compared to the lateral sides (Figure 4A, left; Figure. S5, S6A). PIN3-GFP signal could
262 be detected in epidermal and cortical cells, with significantly stronger signal on transverse
263 membranes compared to lateral sides in the epidermis (Figure 4B, left; Figure. S5, S6B)
264 and exclusively transverse localization in cortical cells (Figure 4C, left). In surface-grown
265 *ktn1-5* mutant seedlings, the polarities of PIN3-GFP and PIN4-GFP were strongly
266 perturbed. Localization of both PIN3 and PIN4 GFP was significantly enhanced at the
267 lateral membranes of epidermal cells in *ktn1-5* compared to WT (Figure. 4A, 4B, middle;
268 Figure. S6A, S6B). Moreover, PIN3-GFP was mislocalized to lateral membranes in
269 cortical cells of *ktn1-5* (Figure 4C, middle). Intriguingly, PIN1-GFP displayed a unique
270 spatially-restricted localization pattern in the WT hook [33]. PIN1-GFP signal could be
271 detected on the plasma membrane only in cells on the concave side (Figure 4E, left). In
272 the *ktn1-5* hook region, however, PIN1-GFP was completely absent from plasma
273 membrane but it could be detected in punctate intracellular structures (Figure 4E, middle).
274 PIN7-GFP signal could be detected only in epidermal cells, which showed nonpolar
275 localization (Figure S5). In contrast to PIN 1, 3 and 4, neither the localization nor the
276 intensity of PIN7 underwent any change in *ktn1-5* (Figure S6C, S6D). We then examined
277 whether mechanical cues can mediate the localization of PIN transporters required to
278 induce hook formation. When grown inside agar, the polarity of PIN4-GFP in epidermis
279 (Figure 4A right; Figure. S6A) and PIN3-GFP in both epidermis (Figure 4B, right; Figure.
280 S6B) and cortex (Figure. 4C, right) was partially but significantly restored in *ktn1-5*.
281 Furthermore, PIN1-GFP signal was now primarily on the plasma membrane of cells on
282 the concave side in *ktn1-5*, resembling the localization pattern seen in WT hooks (Figure.
283 4D, right).
284 Thus, the genetic analysis of *pin* mutants and localization analysis of PINs strongly
285 supports our scenario: mechanical constraints associated with growth in agar would

286 mediate the recruitment (PIN1) and polarity (PIN3, PIN4) of auxin efflux carrier, thereby
287 generating a differential auxin response and differential cell elongation; the resulting
288 mechanical conflicts would be strong enough for CMTs to align with the directions of
289 mechanical stress, and maintain tissue bending, even compensating the absence of the
290 catalyzer of CMT self-organization, katanin.
291

292 **Cellulose microfibril deposition is critical for differential auxin response in the**
293 **hook**

294 As mentioned above, cellulose acts downstream of CMTs to control directional cell
295 growth, through the CMT-CesA nexus [27]. Interestingly, a role for CesA activity in the
296 regulation of PIN1 localization has also been reported [37]. This would put cellulose
297 upstream of the CMT response to mechanical cues, via the formation of differential auxin
298 patterns and resulting mechanical conflicts. This prompted us to investigate whether
299 external cues require cellulose microfibrils for the establishment of PIN polarities and
300 auxin response. First, we investigated whether the cellulose mutants fail to establish the
301 auxin response maxima critical for hook formation. In contrast to WT plants**,** with DR5::
302 Venus-N7 signal only on the concave side, Figure. 5A), the DR5:: Venus-N7 pattern in
303 seedlings of both the cellulose mutants, *any1* and *pom2-8***,** was altered and diffuse
304 (Figure. 5B, 5C) suggesting a defect in establishing an auxin response maxima when
305 cellulose deposition is affected. Analysis of the localization of PIN efflux carriers showed
306 epidermal polarity of PIN3-GFP and PIN4-GFP was significantly reduced in *any1* and
307 *pom2-8* compared to WT (Figure. 5D, 5E, S7A, S7B). PIN3-GFP was also found on lateral
308 membranes of cortical cells in *any1* and *pom2-8* hooks (Figure. 5F), similar to *ktn1-5*
309 seedlings. Looking at PIN1-GFP, we found that**,** similar to *ktn1-5*, GFP signal was absent
310 from plasma membrane but present in intracellular punctate structures (Figure. 5G).
311 These results are consistent with a scenario in which cellulose is required for the polarity
312 of PIN auxin efflux carrier and the resulting auxin response patterns; in that scenario,
313 cellulose would indirectly control the CMT response to external mechanical cues, via its
314 impact on auxin distribution.
315

316 **Signaling mediated by TMK1 and 4 is necessary for mechanosensitive hook**
317 **formation**

318 Two major pathways have been reported to mediate the auxin response in the hook. The
319 transcription factors ARF7/ ARF19 mediate the canonical auxin response pathway, and
320 as a result the *arf7arf19* double mutant displays a strong hook defect [33]. However, we
321 found that the marked hook defects of the *arf7 arf19* double mutant could be rescued by
322 constraining growth in agar gel (Figure. S8A). Furthermore, the *ktn1-5 arf7 arf19* triple
323 mutant displayed a similar response to mechanical cues as the *ktn1-5* single mutant with
324 respect to hook formation (Figure. S8B). This suggests that hook formation in response
325 to mechanical cues does not require ARF7 and ARF19 activity.
326 A recent study suggests that the plasma membrane localized receptor TMK1 is a
327 component of a non-canonical auxin signaling pathway operating in the apical hook [38].
328 Perception of higher levels of auxin causes cleavage and nuclear translocation of a C-
329 terminal fragment of TMK1 specifically on the concave side of the hook, subsequently
330 repressing growth of these cells through stabilization of specific nuclear AUX/ IAA
331 transcription factors. Since neither ARF7 and ARF19 was required for hook formation in
332 response to external mechanical cues, we investigated whether this pathway acts via
333 TMKs.
334 The *tmk1* null mutant displays a defect in hook maintenance but not in hook formation.
335 Nor do the three remaining members of the TMK family cause any appreciable hook
336 phenotypes [38]. However, the functional redundancy between TMK1 and TMK4 [39]
337 prompted us to look into hook formation in the *tmk1tmk4* double mutant. This mutant
338 showed a clear hook formation defect, as well as defects in auxin response asymmetry
339 as visualized with DR5:: Venus-N7. Strikingly, this response could not be rescued by
340 constraining growth in agar gel (Figure. 6A-C). These results strongly suggest that hook
341 formation in response to growth under mechanical constraints depends on the TMK
342 pathway. Taken together, our observations suggest that the components of the non-
343 canonical auxin response pathway, TMK1 and TMK4, act redundantly and are required
344 to mediate bending in response to mechanical cues during hook formation.
345

346 **Discussion**

347 A unique feature of morphogenesis in plants is the postembryonic adaptability to their
348 environment. Formation of the hook during early seedling establishment is an example of
349 such an adaptive response, protecting the fragile shoot apical meristem during soil
350 emergence. In this study we show that asymmetry in cell elongation, the auxin response
351 and CMT behavior drive differential growth during hook formation. Although these
352 responses are absent in the katanin mutant, we demonstrate that katanin only catalyzes
353 this response: external mechanical cues can generate a hook independent of katanin.
354 Recently, an important role of mechanical cues originating from gravitropic bending of the
355 root to the generation of auxin asymmetry has been proposed during hook formation [40].
356 Our results provide support for this suggestion and reveal a scenario involving auxin efflux
357 carriers, and not auxin influx carriers, and in which CMTs react to external mechanical
358 cues and a TMK-dependent auxin response pathway to promote hook formation.
359 Although apical hook formation has been studied extensively as a model for differential
360 cell elongation and underlying hormonal pathways and transcriptional networks [41], most
361 of these studies were performed by growing seeds on the surface of agar. Under these
362 laboratory conditions, the hypocotyl is not subject to external cues akin to mechanical
363 constraints imposed by soil. As a result, the role of exogenous mechanical cues in
364 hypocotyl bending to form a hook has not been explored in detail. By introducing external
365 mechanical cues in the form of agar-grown hypocotyls, we reveal that three key factors,
366 auxin response factors, auxin influx carriers and microtubule-severing enzyme katanin
367 are dispensable for apical hook formation. By challenging the intrinsic genetic control of
368 apical hook formation with external mechanical cues, we could extract the key players of
369 tissue bending in the context of apical hook formation.
370 How plant cells may differentiate between external (e.g. wind, touch) and internal
371 mechanical cues is subject to debate. Plant cells may in fact use the same pathways to
372 respond to mechanical forces, independent of the cause of mechanical stress [42]. In
373 particular, artificial mechanical perturbations are classically performed to check whether
374 plant cells can orient their CMTs with the direction of maximal tensile stress, mimicking
375 the CMT response to growth- and shape-derived stress in control tissues [15, 16, 43].
376 Yet, the associated mechanotransduction pathways have remained unknown so far.

377 Among the candidate mechanisms to exclude, CMTs seem to align with local mechanical
378 stress reorientation in the shoot apical meristem even when calcium signals are blocked
379 [44] or when auxin gradients are largely impaired [45] Therefore it has been proposed
380 that CMTs may be their own mechanosensors [14] echoing what has been proposed for
381 actin in animals [46, 47] and building on evidence from stretched microtubules *in vitro*
382 [48]. Yet, the integration of such behaviors in development requires a coordinator, a role
383 that could be played by auxin and mediated by a TMK dependent, non-canonical auxin
384 response pathway.
385 Several mechanisms mediate the formation of ordered CMT arrays, including
386 polymerization/ depolymerization, bundling and severing [49]. Microtubule severing by
387 katanin has been shown to promote CMT anisotropy in several studies; reviewed in [17]
388 and indeed our data also show that in the absence of katanin, CMT arrays are more
389 isotropic. However, we found that mechanical cues can promote CMT anisotropy in the
390 absence of katanin. At first glance, our observations are in conflict with the role of katanin
391 in mediating the response of CMTs to external mechanical cues [15]. However, our data
392 are consistent with slower but pronounced reorganization of CMTs in meristems of
393 katanin mutants subjected to prolonged mechanical cues [9, 50]. Katanin-independent
394 CMT reorganization can happen by motor protein mediated reorientation of CMTs [51].
395 Also, altered polymerization/ depolymerization of MTs by mechanical stress can
396 rearrange CMTs in absence of katanin activity [52]. Indeed, hypersensitivity of mechanical
397 constrain mediated hook formation in *ktn1-5* seedlings towards MT-depolymerizing and
398 polymerizing drugs (oryzalin and paclitaxel) point towards an important role of microtubule
399 polymerization/ depolymerization in katanin-independent CMT reorganization.
400 CMT disorganization associated with loss of katanin function alters the organization of
401 overlaying cellulose microfibrils [53]; this, together with the alteration of PIN1 polarity
402 associated with cellulose defects [37], raises the possibility that the PIN localization
403 defects seen in the *ktn1-5* mutant stems from cellulose disorganization. That PIN
404 mislocalization is similar in *any1* and *pom2-8* mutants supports the importance of
405 cellulose organization in guiding the PIN polarity necessary for hook formation.
406 Furthermore, it has been reported that PIN1 localization at the plasma membrane is
407 sensitive to mechanical stress [54]. It is conceivable that CMTs and cellulose regulate

408 PIN localization and auxin asymmetry formation indirectly, by mediating mechanical
409 stress associated with tissue folding. Nonetheless, our study reveals that CMTs and
410 cellulose, by acting as mediators of mechanical stress, can guide key developmental
411 processes such as tissue folding in plants by modulating PIN localization and auxin
412 asymmetry. The localization of TMKs at the cell periphery, their role in auxin perception
413 [39] together with their role in apical hook formation, opens the possibility that these
414 receptors may act as an integrator of both biochemical (auxin) and mechanical cues.
415 To conclude, the analysis of apical hook formation in the presence of external mechanical
416 cues are reminiscent of observations in *Drosophila*. During gastrulation, tissue
417 deformation through external mechanical cues can compensate defective myosin in
418 *Drosophila* [4]. Here we find that stiff agar can trigger apical hook formation, even when
419 CMT dynamics is reduced in the katanin mutant. Beyond the parallel between plants and
420 animals, such approaches further show how challenging development with external
421 mechanical cues can be a productive way to dissect the molecular pathways behind
422 morphogenesis, and identify the core players.
423

424 **Acknowledgements:**

425 We thank Eva Benkova, Geoffrey O. Wasteneys, Ranjan Swarup and Enrico Scarpella
426 for sharing published materials. Our sincere thanks to Arun Sampathkumar, Anne-Lise
427 Routier-Kierzkowska, Daniel Kierzkowski and Dolf Weijers for reading through the
428 manuscript and providing valuable inputs. A.B thanks the Wenner-Gren foundation for a
429 travel fellowship.

430 **Author Contributions**

431 A.B, R.B, O.H and M.B conceived the project and designed experiments. E.M performed
432 the MicroCT experiments. B.A contributed the *auxlax* quadruple mutant data. A.B
433 performed all other experiments and analysed the data. K.J contributed to initial screening
434 of the *katanin* mutant phenotypes and provided valuable discussions. T.X provided critical
435 intellectual inputs. S.V provided the Surfcut analysis tool and provided critical inputs. A.B,
436 R.B, O.H and M.B wrote the paper. R.B guided the research.

437 **Declaration of Interests**

438 The authors declare no competing interests

439 **Materials and methods:**

440 **Plant material**

441 Arabidopsis thaliana ecotype Col-0 was used as wild type (WT) control in all experiments.
442 The mutant lines *ktn1-5* [20], *any1* [28], *pom2-8* [29], *tua5*^{D251N} [26], *pin1 3 4 7* [55], *aux1*
443 *lax1 lax2 lax3 [35] arf7arf19 [56] tmk1tmk4 [39] and fluorescent reporter lines 35S:: GFP-*
444 *MAP4 [23], PIN1:: PIN1-GFP, PIN3:: PIN3-GFP [33], PIN4:: PIN4-GFP, PIN7:: PIN7-GFP*
445 [55]*, DR5:: Venus-N7* [34] *lines have been described previously.*

446 *Time lapse analysis of apical hook development*

447 For time lapse imaging of apical hook development, seegs sown on surface of agar plates
448 or emebbeded in agar (1/2 Murashige and Skoog medium, 1% plant agar, Duchefa
449 Biochemie) , were grown on vertical plates in the dark at 21°C illuminated with far infra-
450 red-light (850 nm). Seedlings were photographed every hour using a Canon D50 camera
451 without the infrared filter. Hook angles were measured as previously described [21] using
452 *Image J/Fiji.*

453 **CMT imaging and quantification**

454 Dark-grown WT or ktn1-5 mutant plants expressing GFP-MAP4 were imaged with a Zeiss
455 LSM 880 confocal microscope using airyscan scanning. Postacquisition, the images were
456 processed using the airyscan processing module incorporated in the Zen 2.3 software.
457 The cortical signal (0-10 μm depth) was extracted from the stacks using the Surfcut
458 pipeline incorporated in the Image J/Fiji program [57]. CMT anisotropy was measured
459 using the FibrilTool plugin [24] in Image J/Fiji.

460 **Confocal laser-scanning microscopy and quantification of fluorescence intensity**

461 Samples were imaged using a Ziess LSM 880 confocal laser scanning microscope. GFP,
462 and YFP, were excited by 488 and 514 lasers respectively and respective fluorescence
463 emissions were detected at 492-540 and 518-560 nm windows. Images for plasma
464 membrane fluorescence intensity quantification of PIN1-GFP, PIN3-GFP, PIN4-GFP and

465 PIN7-GFP in hook epidermal cells of were captured under identical acquisition
466 parameters (laser power, photomultiplier gain, offset, zoom, and resolution) between WT
467 and mutants. Polarity index was calculated as the ratio of basal/ lateral intensities.
468 Statistical analysis methods are described in Figureure legends.

469 **X-Ray microcomputed tomography.**

470 WT and *ktn1-5* seeds were buried under 1 cm of sterile, sandy loamy soil. Seedlings were
471 scanned after 6 days post-sowing by X-Ray microcomputed tomography as described
472 previously [25] at 6.5 μm resolution.

473 **References**

474 1. Farge, E. (2003). Mechanical induction of twist in the Drosophila foregut/stomodeal
475 primordium. Current Biology *13*, 1365-1377.
476 2. Martin, A.C., Kaschube, M., and Wieschaus, E.F. (2009). Pulsed contractions of
477 an actin-myosin network drive apical constriction. Nature *457*, 495-U411.
478 3. Sherrard, K., Robin, F., Lemaire, P., and Munro, E. (2010). Sequential Activation
479 of Apical and Basolateral Contractility Drives Ascidian Endoderm Invagination.
480 Current Biology *20*, 1499-1510.
481 4. Pouille, P.A., Ahmadi, P., Brunet, A.C., and Farge, E. (2009). Mechanical Signals
482 Trigger Myosin II Redistribution and Mesoderm Invagination in Drosophila
483 Embryos. Sci Signal *2*.
484 5. Echevin, E., Le Gloanec, C., Skowronska, N., Routier-Kierzkowska, A.L., Burian,
485 A., and Kierzkowski, D. (2019). Growth and biomechanics of shoot organs. J Exp
486 Bot *70*, 3573-3585.
487 6. Chaiwanon, J., Wang, W.F., Zhu, J.Y., Oh, E., and Wang, Z.Y. (2016). Information
488 Integration and Communication in Plant Growth Regulation. Cell *164*, 1257-1268.
489 7. Braam, J. (2005). In touch: plant responses to mechanical stimuli. New Phytol *165*,
490 373-389.
491 8. Kutschera, U., and Nikas, K.J. (2007). The epidermal-growth-control theory of
492 stem elongation: An old and a new perspective. J Plant Physiol *164*, 1395-1409.
493 9. Uyttewaal, M., Burian, A., Alim, K., Landrein, B.T., Borowska-Wykret, D., Dedieu,
494 A., Peaucelle, A., Ludynia, M., Traas, J., Boudaoud, A., et al. (2012). Mechanical
495 Stress Acts via Katanin to Amplify Differences in Growth Rate between Adjacent
496 Cells in Arabidopsis. Cell *149*, 439-451.
497 10. Hervieux, N., Tsugawa, S., Fruleux, A., Dumond, M., Routier-Kierzkowska, A.L.,
498 Komatsuzaki, T., Boudaoud, A., Larkin, J.C., Smith, R.S., Li, C.B., et al. (2017).
499 Mechanical Shielding of Rapidly Growing Cells Buffers Growth Heterogeneity and
500 Contributes to Organ Shape Reproducibility. Current Biology *27*, 3468-+.
501 11. Huang, C.J., Wang, Z.L., Quinn, D., Suresh, S., and Hsia, K.J. (2018). Differential
502 growth and shape formation in plant organs. P Natl Acad Sci USA *115*, 12359-
503 12364.

504 12. Abbas, M., Alabadi, D., and Blazquez, M.A. (2013). Differential growth at the apical
505 hook: all roads lead to auxin. Front Plant Sci *4*.
506 13. Landrein, B., Kiss, A., Sassi, M., Chauvet, A., Das, P., Cortizo, M., Laufs, P.,
507 Takeda, S., Aida, M., Traas, J., et al. (2015). Mechanical stress contributes to the
508 expression of the STM homeobox gene in Arabidopsis shoot meristems. Elife *4*.
509 14. Hamant, O., Inoue, D., Bouchez, D., Dumais, J., and Mjolsness, E. (2019). Are
510 microtubules tension sensors? Nat Commun *10*.
511 15. Sampathkumar, A., Krupinski, P., Wightman, R., Milani, P., Berquand, A.,
512 Boudaoud, A., Hamant, O., Jonsson, H., and Meyerowitz, E.M. (2014). Subcellular
513 and supracellular mechanical stress prescribes cytoskeleton behavior in
514 Arabidopsis cotyledon pavement cells. Elife *3*.
515 16. Robinson, S., and Kuhlemeier, C. (2018). Global Compression Reorients Cortical
516 Microtubules in Arabidopsis Hypocotyl Epidermis and Promotes Growth. Current
517 Biology *28*, 1794-+.
518 17. Luptovciak, I., Komis, G., Takac, T., Ovecka, M., and Samaj, J. (2017). Katanin: A
519 Sword Cutting Microtubules for Cellular, Developmental, and Physiological
520 Purposes. Front Plant Sci *8*.
521 18. Bouquin, T., Mattsson, O., Naested, H., Foster, R., and Mundy, J. (2003). The
522 Arabidopsis lue1 mutant defines a katanin p60 ortholog involved in hormonal
523 control of microtubule orientation during cell growth. J Cell Sci *116*, 791-801.
524 19. Chakrabortty, B., Blilou, I., Scheres, B., and Mulder, B.M. (2018). A computational
525 framework for cortical microtubule dynamics in realistically shaped plant cells. Plos
526 Comput Biol *14*.
527 20. Lin, D., Cao, L., Zhou, Z., Zhu, L., Ehrhardt, D., Yang, Z., and Fu, Y. (2013). Rho
528 GTPase signaling activates microtubule severing to promote microtubule ordering
529 in Arabidopsis. Curr Biol *23*, 290-297.
530 21. Boutte, Y., Jonsson, K., McFarlane, H.E., Johnson, E., Gendre, D., Swarup, R.,
531 Friml, J., Samuels, L., Robert, S., and Bhalerao, R.P. (2013). ECHIDNA-mediated
532 post-Golgi trafficking of auxin carriers for differential cell elongation. Proc Natl Acad
533 Sci U S A *110*, 16259-16264.
534 22. Ikushima, T., and Shimmen, T. (2005). Mechano-sensitive orientation of cortical
535 microtubules during gravitropism in azuki bean epicotyls. J Plant Res *118*, 19-26.
536 23. Marc, J., Granger, C.L., Brincat, J., Fisher, D.D., Kao, T.H., McCubbin, A.G., and
537 Cyr, R.J. (1998). A GFP-MAP4 reporter gene for visualizing cortical microtubule
538 rearrangements in living epidermal cells. Plant Cell *10*, 1927-1939.
539 24. Boudaoud, A., Burian, A., Borowska-Wykret, D., Uyttewaal, M., Wrzalik, R.,
540 Kwiatkowska, D., and Hamant, O. (2014). FibrilTool, an ImageJ plug-in to quantify
541 fibrillar structures in raw microscopy images. Nat Protoc *9*, 457-463.
542 25. Orman-Ligeza, B., Morris, E.C., Parizot, B., Lavigne, T., Babe, A., Ligeza, A., Klein,
543 S., Sturrock, C., Xuan, W., Novak, O., et al. (2018). The Xerobranching Response
544 Represses Lateral Root Formation When Roots Are Not in Contact with Water.
545 Current Biology *28*, 3165-+.
546 26. Ishida, T., Kaneko, Y., Iwano, M., and Hashimoto, T. (2007). Helical microtubule
547 arrays in a collection of twisting tubulin mutants of Arabidopsis thaliana. P Natl
548 Acad Sci USA *104*, 8544-8549.

549 27. Paredez, A.R., Somerville, C.R., and Ehrhardt, D.W. (2006). Visualization of
550 cellulose synthase demonstrates functional association with microtubules. Science
551 *312*, 1491-1495.
552 28. Fujita, M., Himmelspach, R., Ward, J., Whittington, A., Hasenbein, N., Liu, C.,
553 Truong, T.T., Galway, M.E., Mansfield, S.D., Hocart, C.H., et al. (2013). The
554 anisotropy1 D604N Mutation in the Arabidopsis Cellulose Synthase1 Catalytic
555 Domain Reduces Cell Wall Crystallinity and the Velocity of Cellulose Synthase
556 Complexes. Plant Physiol *162*, 74-85.
557 29. Bringmann, M., Li, E.Y., Sampathkumar, A., Kocabek, T., Hauser, M.T., and
558 Persson, S. (2012). POM-POM2/CELLULOSE SYNTHASE INTERACTING1 Is
559 Essential for the Functional Association of Cellulose Synthase and Microtubules in
560 Arabidopsis. Plant Cell *24*, 163-177.
561 30. DeBolt, S., Gutierrez, R., Ehrhardt, D.W., and Somerville, C. (2007). Nonmotile
562 cellulose synthase subunits repeatedly accumulate within localized regions at the
563 plasma membrane in Arabidopsis hypocotyl cells following 2,6-dichlorobenzonitrile
564 treatment. Plant Physiol *145*, 334-338.
565 31. Raz, V., and Koornneef, M. (2001). Cell division activity during apical hook
566 development. Plant Physiol *125*, 219-226.
567 32. Zadnikova, P., Wabnik, K., Abuzeineh, A., Gallemi, M., Van Der Straeten, D.,
568 Smith, R.S., Inze, D., Friml, J., Prusinkiewicz, P., and Benkova, E. (2016). A Model
569 of Differential Growth-Guided Apical Hook Formation in Plants. Plant Cell *28*,
570 2464-2477.
571 33. Zadnikova, P., Petrasek, J., Marhavy, P., Raz, V., Vandenbussche, F., Ding, Z.J.,
572 Schwarzerova, K., Morita, M.T., Tasaka, M., Hejatko, J., et al. (2010). Role of PIN-
573 mediated auxin efflux in apical hook development of Arabidopsis thaliana.
574 Development *137*, 607-617.
575 34. Heisler, M.G., Ohno, C., Das, P., Sieber, P., Reddy, G.V., Long, J.A., and
576 Meyerowitz, E.M. (2005). Patterns of auxin transport and gene expression during
577 primordium development revealed by live imaging of the Arabidopsis inflorescence
578 meristem. Current Biology *15*, 1899-1911.
579 35. Vandenbussche, F., Petrasek, J., Zadnikova, P., Hoyerova, K., Pesek, B., Raz, V.,
580 Swarup, R., Bennett, M., Zazimalova, E., Benkova, E., et al. (2010). The auxin
581 influx carriers AUX1 and LAX3 are involved in auxin-ethylene interactions during
582 apical hook development in Arabidopsis thaliana seedlings. Development *137*,
583 597-606.
584 36. Grunewald, W., and Friml, J. (2010). The march of the PINs: developmental
585 plasticity by dynamic polar targeting in plant cells. Embo J *29*, 2700-2714.
586 37. Feraru, E., Feraru, M.I., Kleine-Vehn, J., Martiniere, A., Mouille, G., Vanneste, S.,
587 Vernhettes, S., Runions, J., and Friml, J. (2011). PIN Polarity Maintenance by the
588 Cell Wall in Arabidopsis. Current Biology *21*, 338-343.
589 38. Cao, M., Chen, R., Li, P., Yu, Y.Q., Zheng, R., Ge, D.F., Zheng, W., Wang, X.H.,
590 Gu, Y.T., Gelova, Z., et al. (2019). TMK1-mediated auxin signalling regulates
591 differential growth of the apical hook. Nature *568*, 240-+.
592 39. Dai, N., Wang, W.Y., Patterson, S.E., and Bleecker, A.B. (2013). The TMK
593 Subfamily of Receptor-Like Kinases in Arabidopsis Display an Essential Role in
594 Growth and a Reduced Sensitivity to Auxin. Plos One *8*.

595 40. Zhu, Q., Gallemi, M., Pospisil, J., Zadnikova, P., Strnad, M., and Benkova, E.
596 (2019). Root gravity response module guides differential growth determining both
597 root bending and apical hook formation in Arabidopsis. Development *146*.
598 41. Mazzella, M.A., Casal, J.J., Muschietti, J.P., and Fox, A.R. (2014). Hormonal
599 networks involved in apical hook development in darkness and their response to
600 light. Front Plant Sci *5*.
601 42. Hamant, O., and Haswell, E.S. (2017). Life behind the wall: sensing mechanical
602 cues in plants. Bmc Biol *15*.
603 43. Hamant, O., Heisler, M.G., Jonsson, H., Krupinski, P., Uyttewaal, M., Bokov, P.,
604 Corson, F., Sahlin, P., Boudaoud, A., Meyerowitz, E.M., et al. (2008).
605 Developmental Patterning by Mechanical Signals in Arabidopsis. Science *322*,
606 1650-1655.
607 44. Li, T., Yan, A., Bhatia, N., Altinok, A., Afik, E., Durand-Smet, P., Tarr, P.T.,
608 Schroeder, J.I., Heisler, M.G., and Meyerowitz, E.M. (2019). Calcium signals are
609 necessary to establish auxin transporter polarity in a plant stem cell niche. Nat
610 Commun *10*.
611 45. Heisler, M.G., Hamant, O., Krupinski, P., Uyttewaal, M., Ohno, C., Jonsson, H.,
612 Traas, J., and Meyerowitz, E.M. (2010). Alignment between PIN1 Polarity and
613 Microtubule Orientation in the Shoot Apical Meristem Reveals a Tight Coupling
614 between Morphogenesis and Auxin Transport. Plos Biol *8*.
615 46. Risca, V.I., Wang, E.B., Chaudhuri, O., Chia, J.J., Geissler, P.L., and Fletcher,
616 D.A. (2012). Actin filament curvature biases branching direction. P Natl Acad Sci
617 USA *109*, 2913-2918.
618 47. Yu, M., Yuan, X., Lu, C., Le, S.M., Kawamura, R., Efremov, A.K., Zhao, Z.H.,
619 Kozlov, M.M., Sheetz, M., Bershadsky, A., et al. (2017). mDia1 senses both force
620 and torque during F-actin filament polymerization. Nat Commun *8*.
621 48. Franck, A.D., Powers, A.F., Gestaut, D.R., Gonen, T., Davis, T.N., and Asbury,
622 C.L. (2007). Tension applied through the Dam1 complex promotes microtubule
623 elongation providing a direct mechanism for length control in mitosis. Nat Cell Biol
624 *9*, 832-U171.
625 49. Dixit, R., and Cyr, R. (2004). Encounters between dynamic cortical microtubules
626 promote ordering of the cortical array through angle-dependent modifications of
627 microtubule behavior. Plant Cell *16*, 3274-3284.
628 50. Louveaux, M., Rochette, S., Beauzamy, L., Boudaoud, A., and Hamant, O. (2016).
629 The impact of mechanical compression on cortical microtubules in Arabidopsis: a
630 quantitative pipeline. Plant J *88*, 328-342.
631 51. Inoue, D., Nitta, T., Kabir, A.M.R., Sada, K., Gong, J.P., Konagaya, A., and
632 Kakugo, A. (2016). Sensing surface mechanical deformation using active probes
633 driven by motor proteins. Nat Commun *7*.
634 52. Trushko, A., Schaffer, E., and Howard, J. (2013). The growth speed of
635 microtubules with XMAP215-coated beads coupled to their ends is increased by
636 tensile force. P Natl Acad Sci USA *110*, 14670-14675.
637 53. Burk, D.H., and Ye, Z.H. (2002). Alteration of oriented deposition of cellulose
638 microfibrils by mutation of a katanin-like microtubule-severing protein. Plant Cell
639 *14*, 2145-2160.

640 54. Nakayama, N., Smith, R.S., Mandel, T., Robinson, S., Kimura, S., Boudaoud, A.,
641 and Kuhlemeier, C. (2012). Mechanical Regulation of Auxin-Mediated Growth.
642 Current Biology *22*, 1468-1476.
643 55. Belteton, S.A., Sawchuk, M.G., Donohoe, B.S., Scarpella, E., and Szymanski, D.B.
644 (2018). Reassessing the Roles of PIN Proteins and Anticlinal Microtubules during
645 Pavement Cell Morphogenesis. Plant Physiol *176*, 432-449.
646 56. Okushima, Y., Overvoorde, P.J., Arima, K., Alonso, J.M., Chan, A., Chang, C.,
647 Ecker, J.R., Hughes, B., Lui, A., Nguyen, D., et al. (2005). Functional genomic
648 analysis of the AUXIN RESPONSE FACTOR gene family members in Arabidopsis
649 thaliana: Unique and overlapping functions of ARF7 and ARF19. Plant Cell *17*,
650 444-463.
651 57. Erguvan, O., Louveaux, M., Hamant, O., and Verger, S. (2019). ImageJ SurfCut:
652 a user-friendly pipeline for high-throughput extraction of cell contours from 3D
653 image stacks. Bmc Biol *17*.

654

655

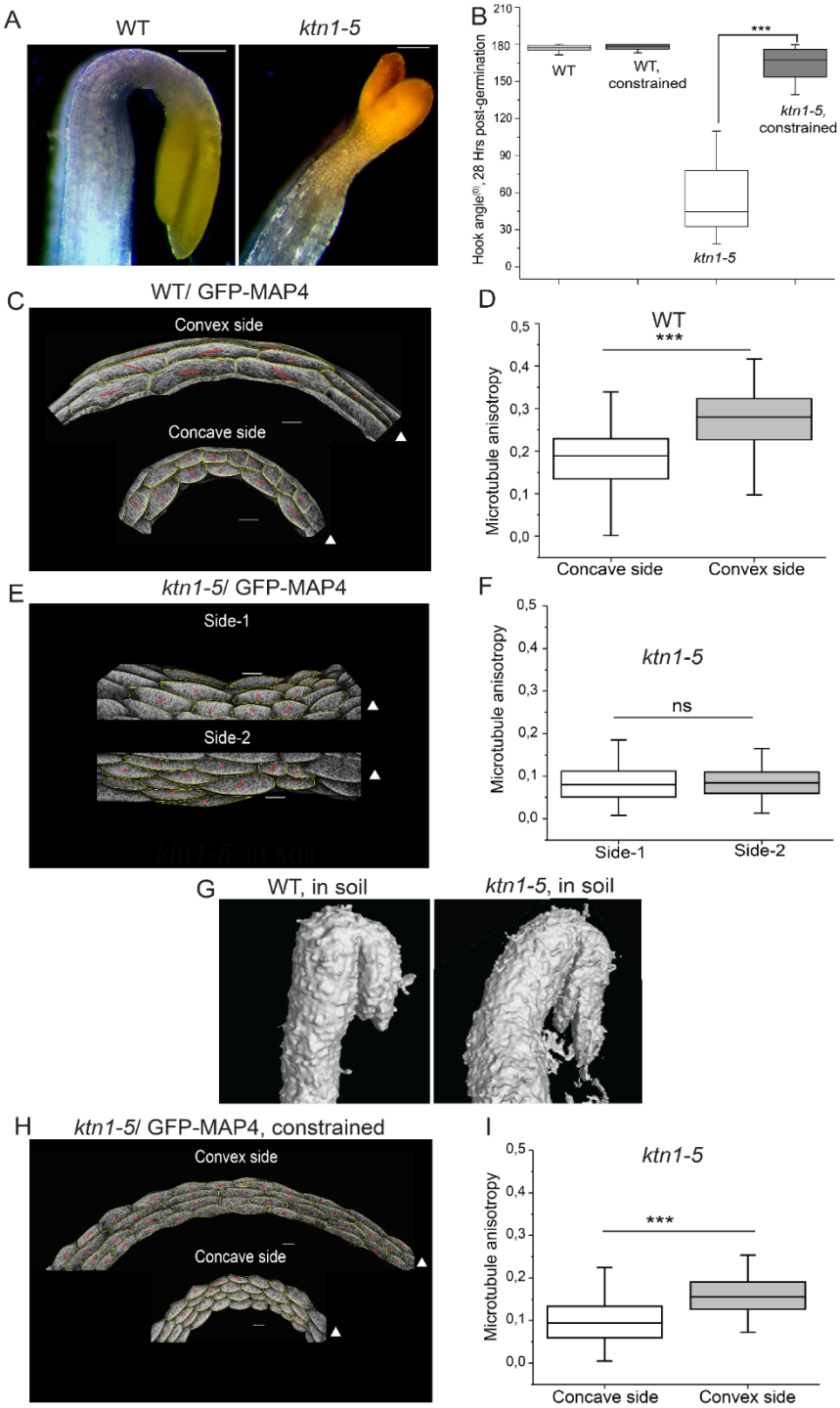

Fig. 1 The *ktn1-5* mutant has a pronounced apical hook defect, which can be rectified by mechanical constraint of soil. (A) Representative image of WT and *ktn1-5* seedlings grown without mechanical constraint 30 Hrs after germination. (B) Quantification of apical-hook angles in WT and *ktn1-5* seedlings growing on the surface of MS agar or growing through the gel (constrained), 28 Hrs after germination, n = 20 seedlings. (C-F) CMT organization in the hook region (0-400 µm from the shoot apical meristem) of WT and *ktn1-5* seedlings. Representative image of CMTs visualized with GFP-MAP4 (C, E). The lengths of the red lines in each cell represent the average CMT anisotropy of the cell quantified by FibrilTool. Triangles denote the end of the hypocotyl with the shoot apical meristem. Quantification of CMT anisotropy values (D, F) across two sides of the hypocotyl measured by FibrilTool. Anisotropy values from at least 150 cells from 5 seedlings were quantified per group. (G) Representative image of soil-embedded WT and *ktn1-5* seedling. Seeds were buried under 1 cm of sandy loamy soil and imaged by micro CT, 6 days after sowing. (H-I) CMT organization in the hook region of *ktn1-5* seedlings grown in the presence of mechanical constraint (inside agar); representative image (H) and anisotropy calculation using FibrilTool (I). The data in C, D, F, and I are plotted as box plots showing the first and third quartiles, split by the median; whiskers extend to minimum and maximum values. Asterisks (***) indicate $P < 0.0001$ (Student's two tailed t-test). Scale bar = 200 µm in A and 20 µm in D, E, F.

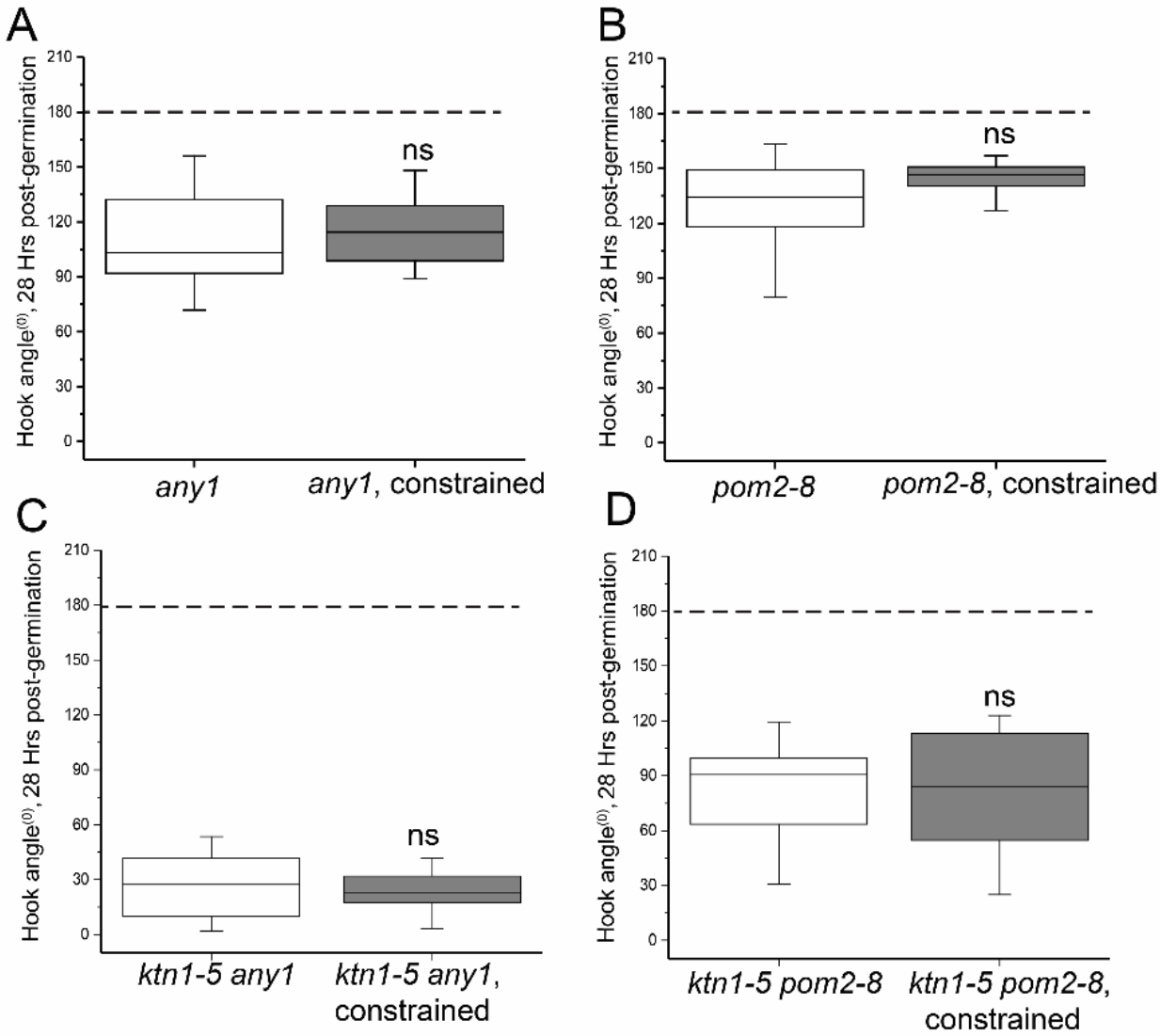

Fig. 2 Hook formation defects in cellulose organization mutants is not rectified by mechanical constrain. Quantification of apical-hook angles in *any1* (A) and *pom2-8* seedlings (B) growing on the surface of MS agar or growing through the gel (constrained), 28 Hrs after germination, n = 20 seedlings. (C-D) Quantification of apical hook angles in *ktn1-5 any1* (C) and *ktn1-5 pom2-8* (D) double mutant seedlings. 28 Hrs after germination, n = 16 seedlings. The data in is plotted as box plots showing the first and third quartiles, split by the median; whiskers extended to minimum and maximum values. The dashed line denotes hook angle of 180^0. ns = non-significant at $P \leq 0.05$ (Student's two tailed t-test).

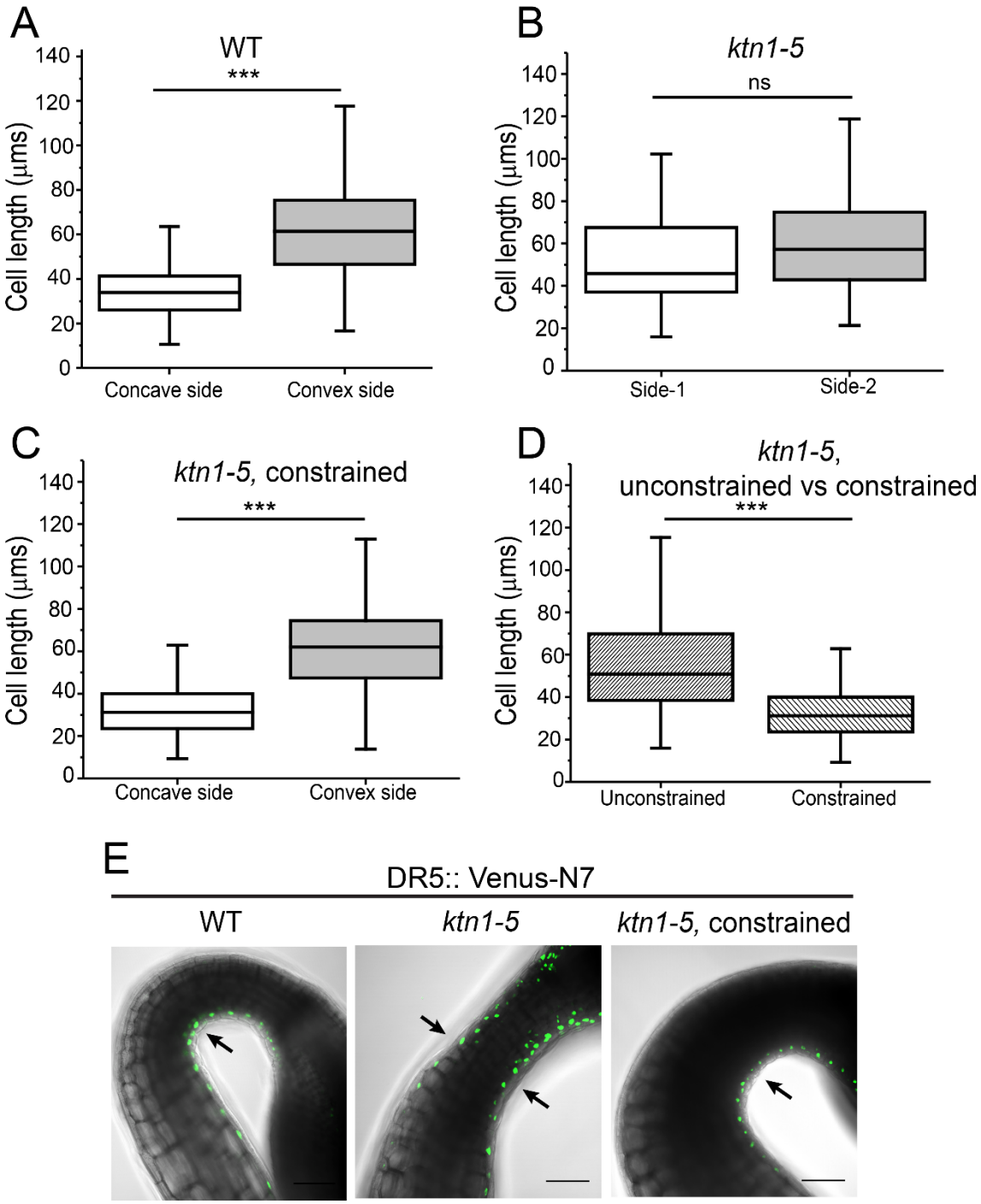

Fig. 3 Mechanical constraint reestablishes auxin response maxima and cell length repression in *ktn1-5* seedlings. (A-C) Quantification of cell length in WT (A), *ktn1-5* (B) and mechanically constrained *ktn1-5* seedlings (C) in the hook region (0-400 µm from the shoot apical meristem). Cell length was measured on at least 150 cells from 5 seedlings per group, where cell outlines were marked with GFP-MAP4. (D) Comparison of average cell length in the hook region of unconstrained *ktn1-5* seedlings with that of concave side cells in constrained *ktn1-5* seedlings shows the reestablishment of cell growth repression by mechanical constraint. Box plots show the first and third quartiles, split by the median; whiskers extend to minimum and maximum values. Asterisks (***) indicate $P < 0.0001$, ns = non-significant at $P \leq 0.05$ (Student's two tailed t-test). (E) Representative image of DR5:: Venus-N7 signal in WT and *ktn1-5* seedlings, 28-30 Hrs post germination. In WT, DR5:: Venus-N7 signal is detected only in epidermal cells on the concave side of the apical hook (arrow). In *ktn1-5*, DR5:: Venus-N7 signal is seen on both sides of the hypocotyl (arrows) suggesting a defect in auxin asymmetry establishment. DR5:: Venus-N7 signal asymmetry is reestablished in *ktn1-5* by mechanical constraint imposed by growing inside agar. Scale bar = 100 µm.

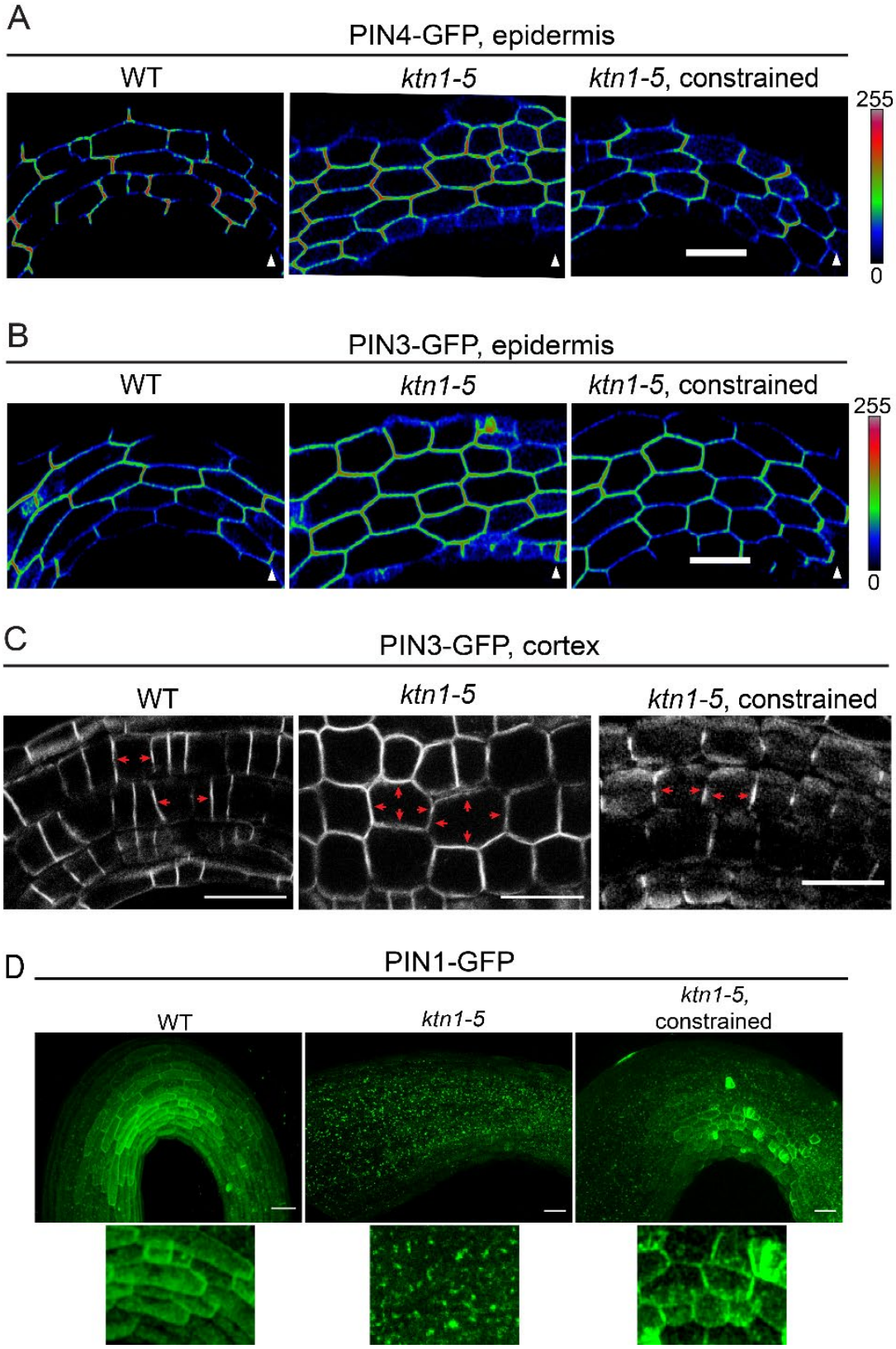

Fig. 4 Altered localization of PIN auxin transporters in *ktn1-5* could be rectified by mechanical constraint. Representative images of PIN4-GFP in epidermis (A), PIN3-GFP in epidermis (B) and PIN3-GFP in cortex (C) in WT, *ktn1-5* and mechanically constrained *ktn1-5* seedlings. (D) PIN1-GFP in WT hook (left) shows plasma membrane localization only on the concave side of the hook. In *ktn1-5* seedlings PIN1-GFP is absent from the plasma membrane (middle). In mechanically constrained *ktn1-5* seedlings, PIN1-GFP is seen on the plasma membrane on cells on the concave side (right). Magnified images of concave side cells are shown underneath. Scale bar = 50 µm. Color bars in (A) and (B) represent 8-bit intensity range of 0-255.

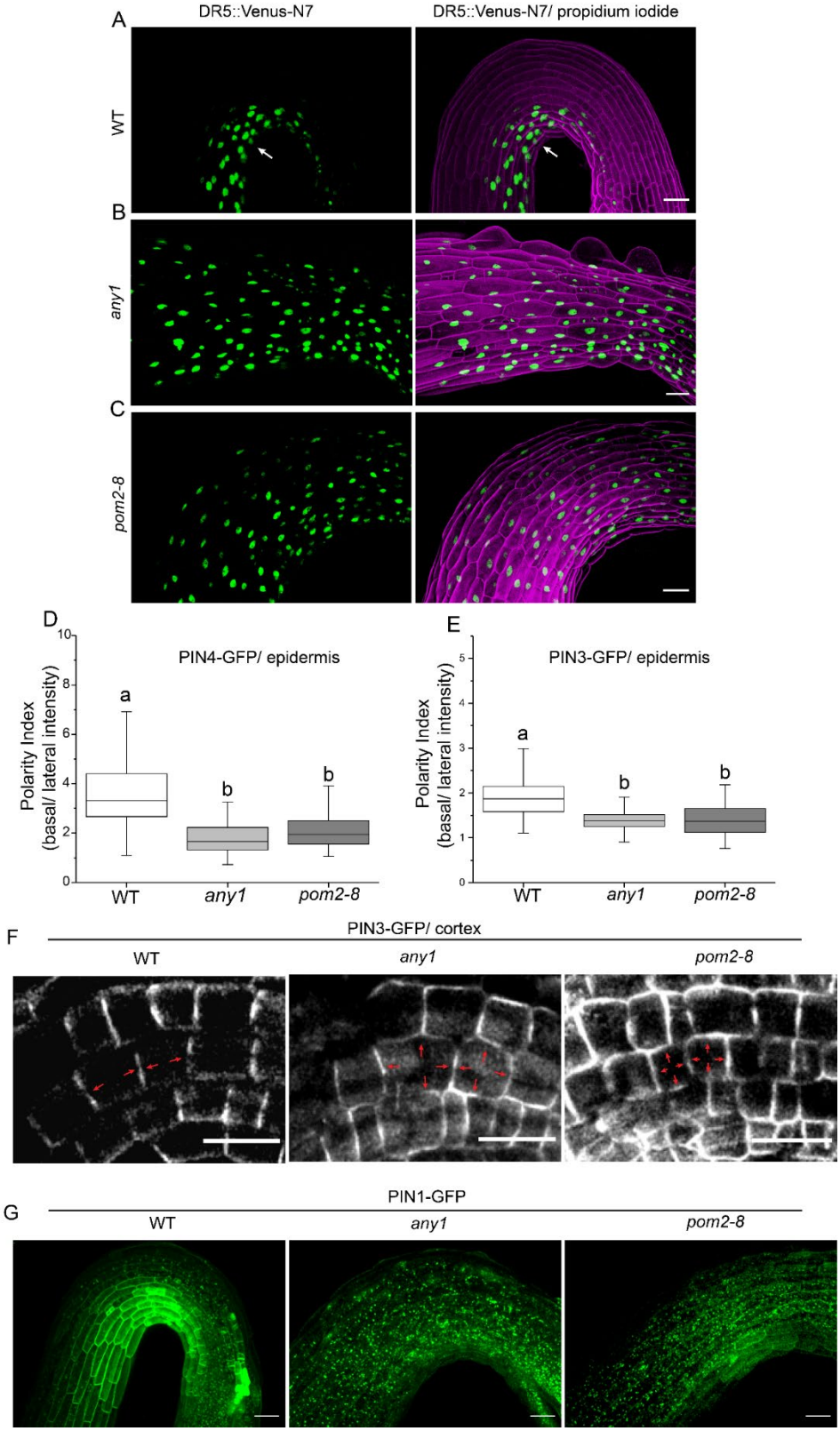

Fig. 5 Altered auxin response asymmetry and PIN localization in cellulose mutants. (A-C) Representative image showing Z-projection of DR5:: Venus-N7 signal in WT (A), any1 (B) and pom2-8 (C) seedlings. The cells are counterstained with propidium iodide. The concave side specific localization of DR5: Venus signal seen in WT (arrow) is altered in any1 and pom2-8 Scale bar = 50 µm. (D-E) Quantification of polarity index (basal/ lateral fluorescence intensity) of PIN4-GFP (D) and PIN3-GFP (E) in epidermal cells of hook region of WT, any1 and pom2-8 seedlings. Polarity index was measured from at least 100 cells from 10 seedlings/ group. Box plots show the first and third quartiles, split by the median; whiskers extended to minimum and maximum values. Groups with significant difference by one-way ANOVA with post hoc Tukey's test ($P < 0.05$) are indicated by different letters. (F) Representative images showing localization of PIN3-GFP in hook region cortical cells of WT, any1 and pom2-8 seedlings. (G) Localization of PIN1-GFP in WT, any1 and pom2-8 seedlings. Scale bar = 50µm. See also Fig. S7.

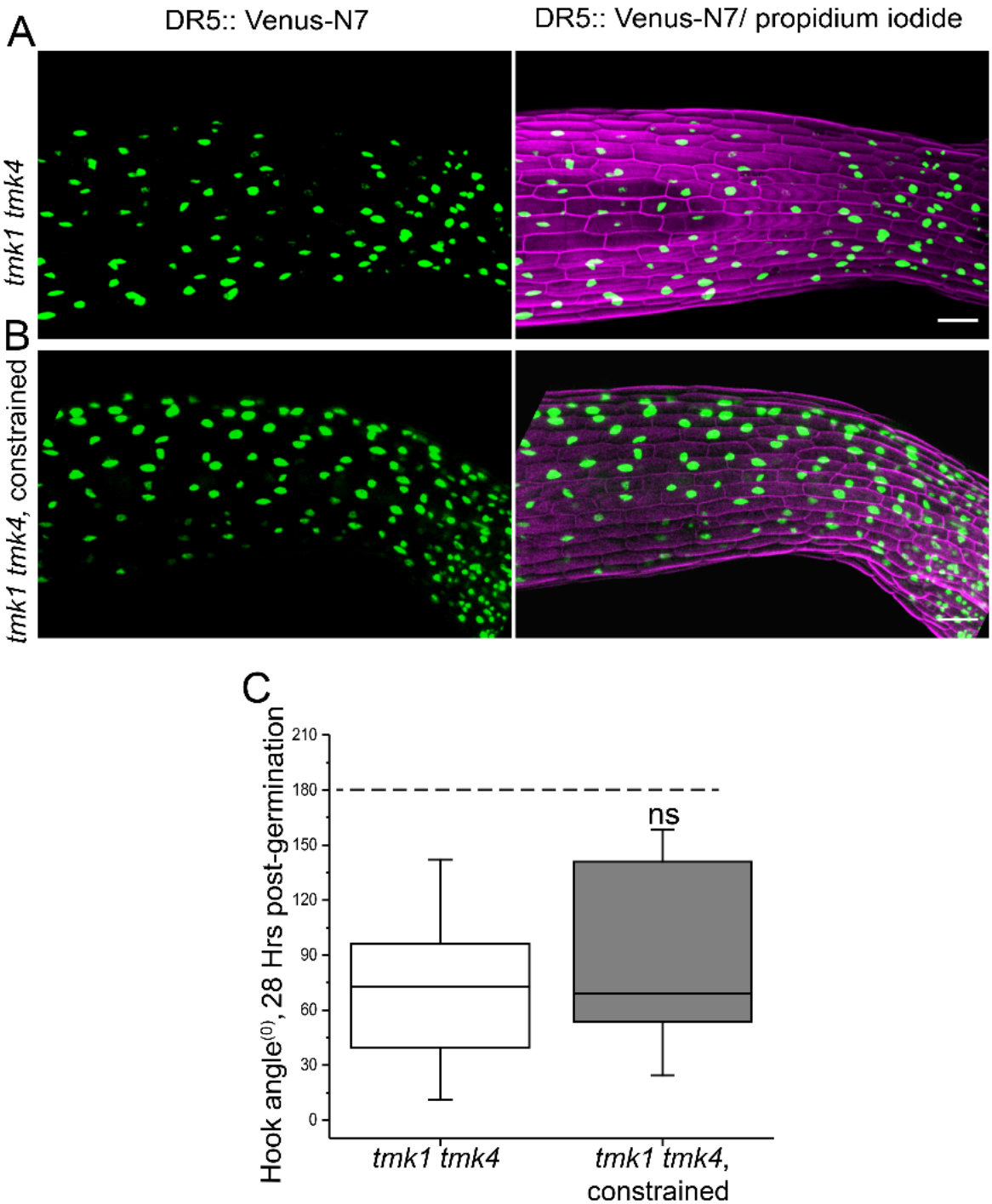

Fig. 6 TMK1 and TMK4 is required for hook formation under mechanical constrain. Representative image showing Z-projection of DR5::Venus-N7 signal in *tmk1tmk4* seedling in absence (A) and in presence of mechanical constrain (B). The cells are counterstained with propidium iodide, Scale bar = 50 µm. (C) Quantification of apical-hook angles in *tmk1 tmk4* growing on the surface of MS agar or growing through the gel (constrained), 28 Hrs after germination, n = 16 seedlings. Box plots show the first and third quartiles, split by the median; whiskers extended to minimum and maximum values. The dashed line denotes hook angle of 180^0. ns = non-significant at $P \leq 0.05$ (Student's two tailed t-test).

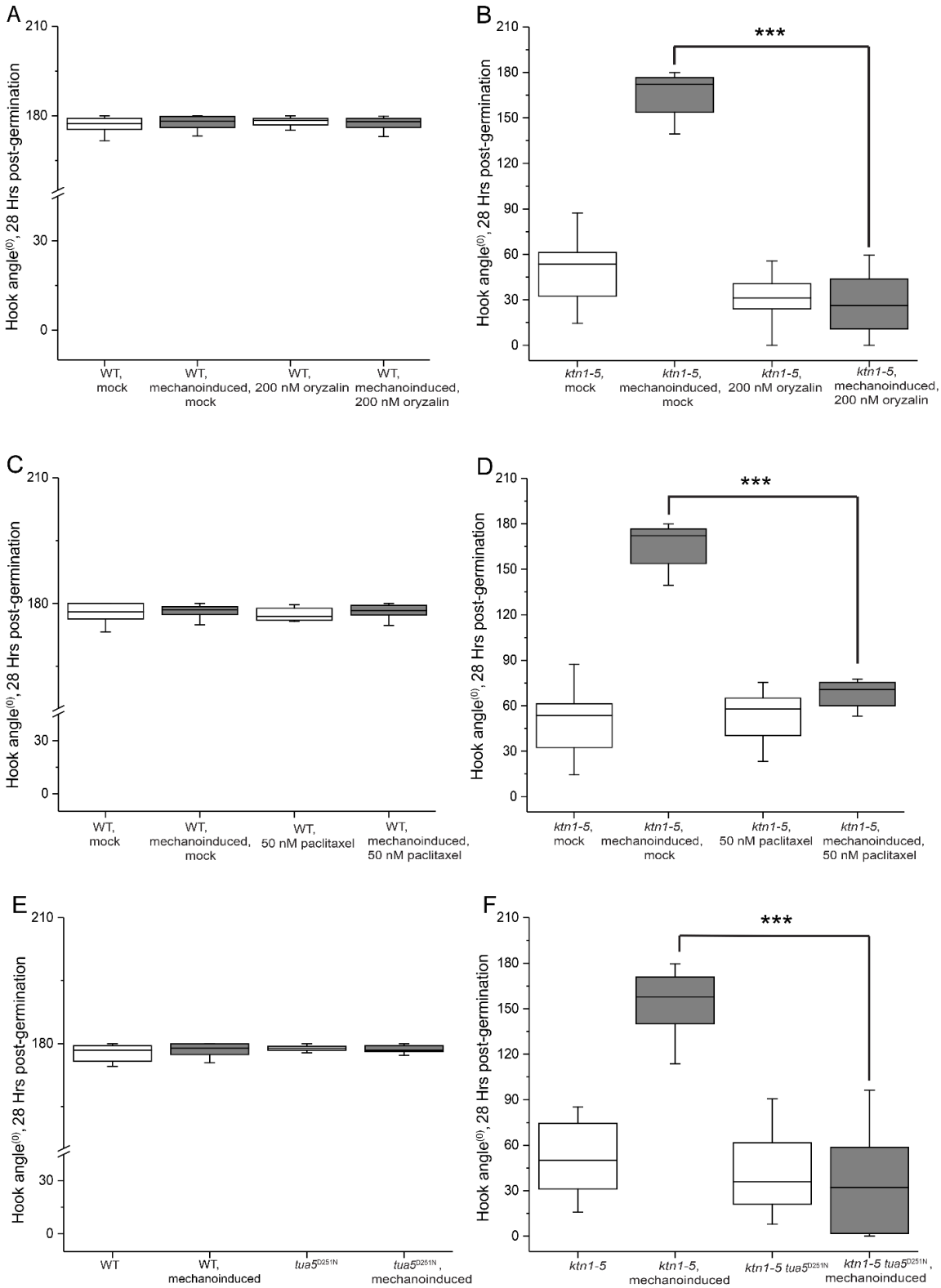

Fig. S1 Chemical and genetic perturbations of microtubules eliminate mechanically-constrained hook formation in the *ktn1-5* mutant. Quantification of apical hook angles in WT and *ktn1-5* seedlings (in the presence and absence of mechanical constraint) treated with 200 nM oryzalin (A, B) or 50 nM paclitaxel (C, D) or in the presence of the *tua5*^{D251N} mutation (E, F), 28 Hrs post-germination. n = 18 seedlings per group, box plots showing the first and third quartiles, split by the median; whiskers extend to minimum and maximum values. Indicated groups are compared by Student's two tailed t-test, asterisks (***) indicate $P < 0.0001$.

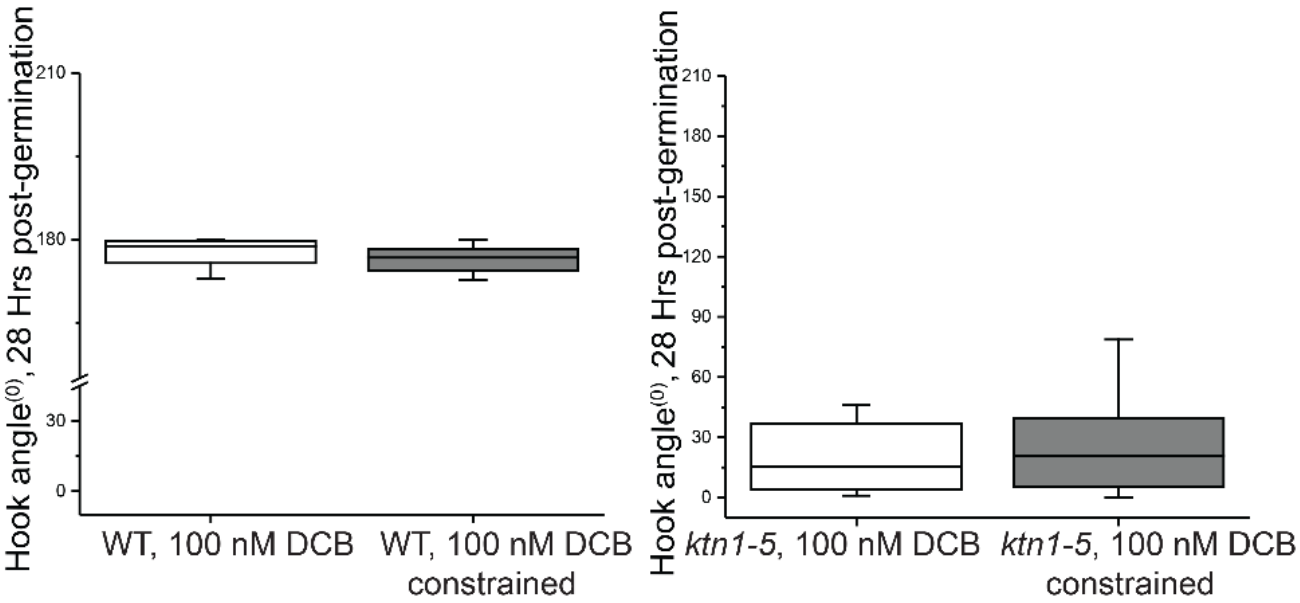

Fig. S2 Mechanically constrained hook formation in *ktn1-5* is hypersensitive to the cellulose biosynthesis inhibitor DCB. Quantification of apical-hook angles in WT (A) and *ktn1-5* (B) treated with 100 nM DCB in the absence or presence of mechanical constraint, 28 Hrs after germination. n = 16 seedlings/ group.

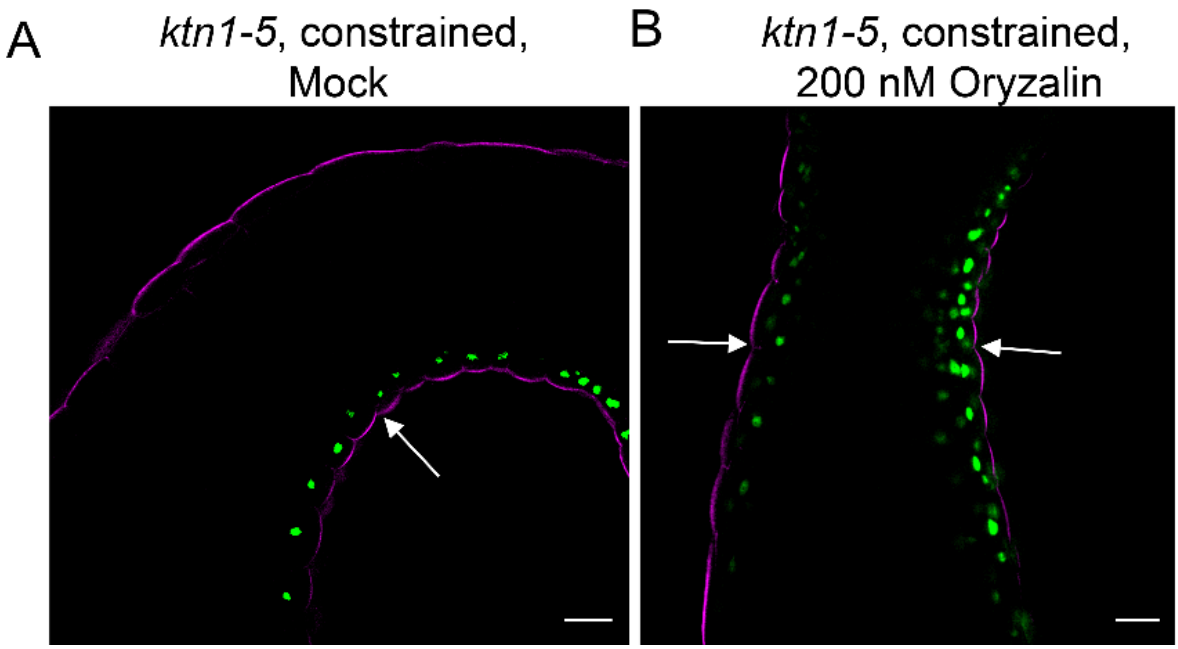

Fig. S3 Representative image of DR5:: Venus-N7 signal in mechanically constrained *ktn1-5* seedlings grown inside mock MS agar (A) or MS agar supplemented with 200 nM Oryzalin (B). The seedlings are counterstained with propidium iodide. DR5:: Venus-N7 signal is indicated by arrows. At least 10 seedlings were observed per group.

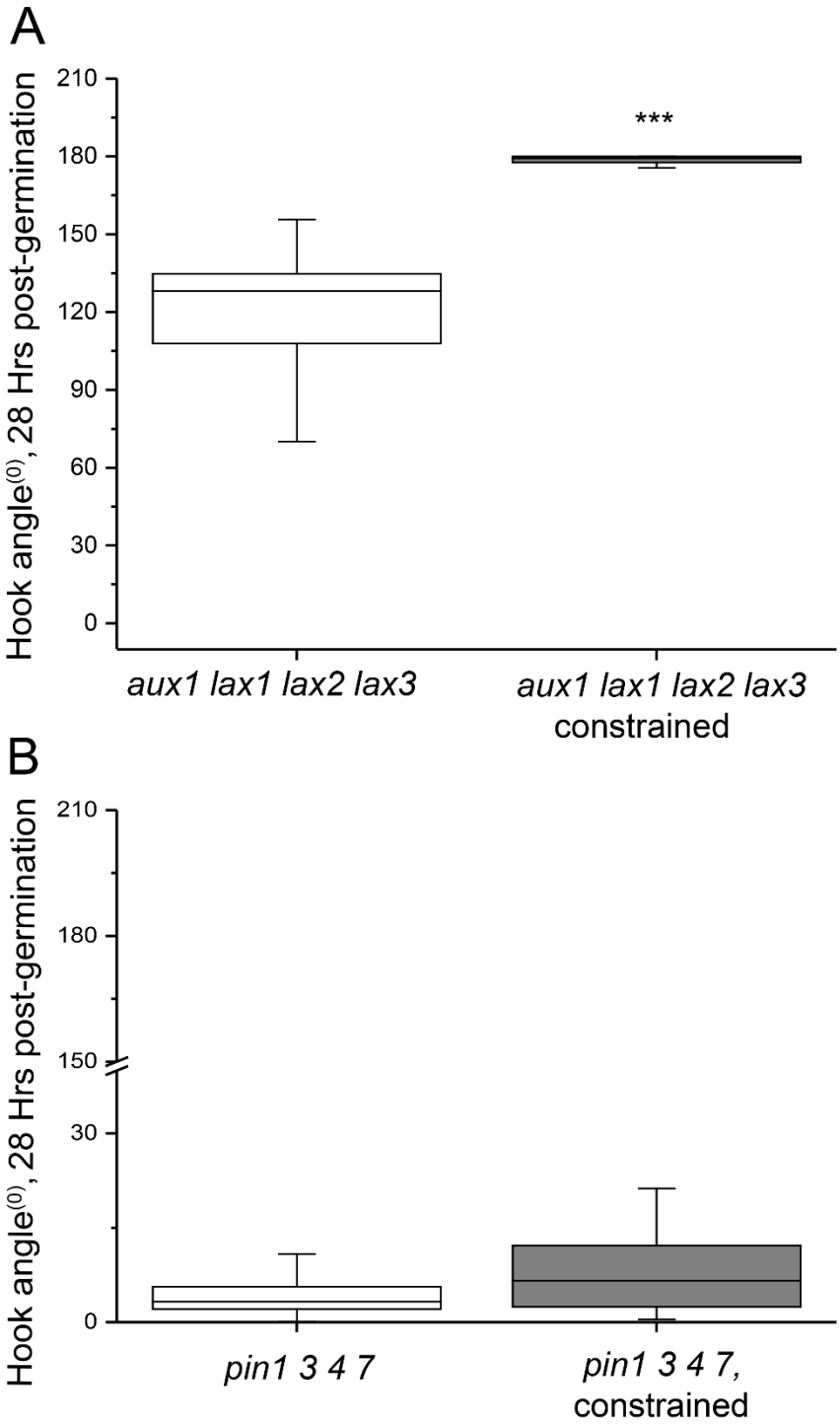

Fig. S4 Involvement of auxin carriers in mechanically constrained hook formation. Quantification of apical-hook angles in *aux1 lax1 lax2 lax3* quadruple mutant (A) and *pin1 3 4 7* quadruple mutant (B) growing on the surface of MS agar or growing through the gel (constrained), 28 Hrs after germination, n = 16 seedlings/ group. Box plots showing the first and third quartiles, split by the median; whiskers extend to minimum and maximum values. Indicated groups are compared by Student's two tailed t-test, asterisks (***) indicate $P < 0.0001$.

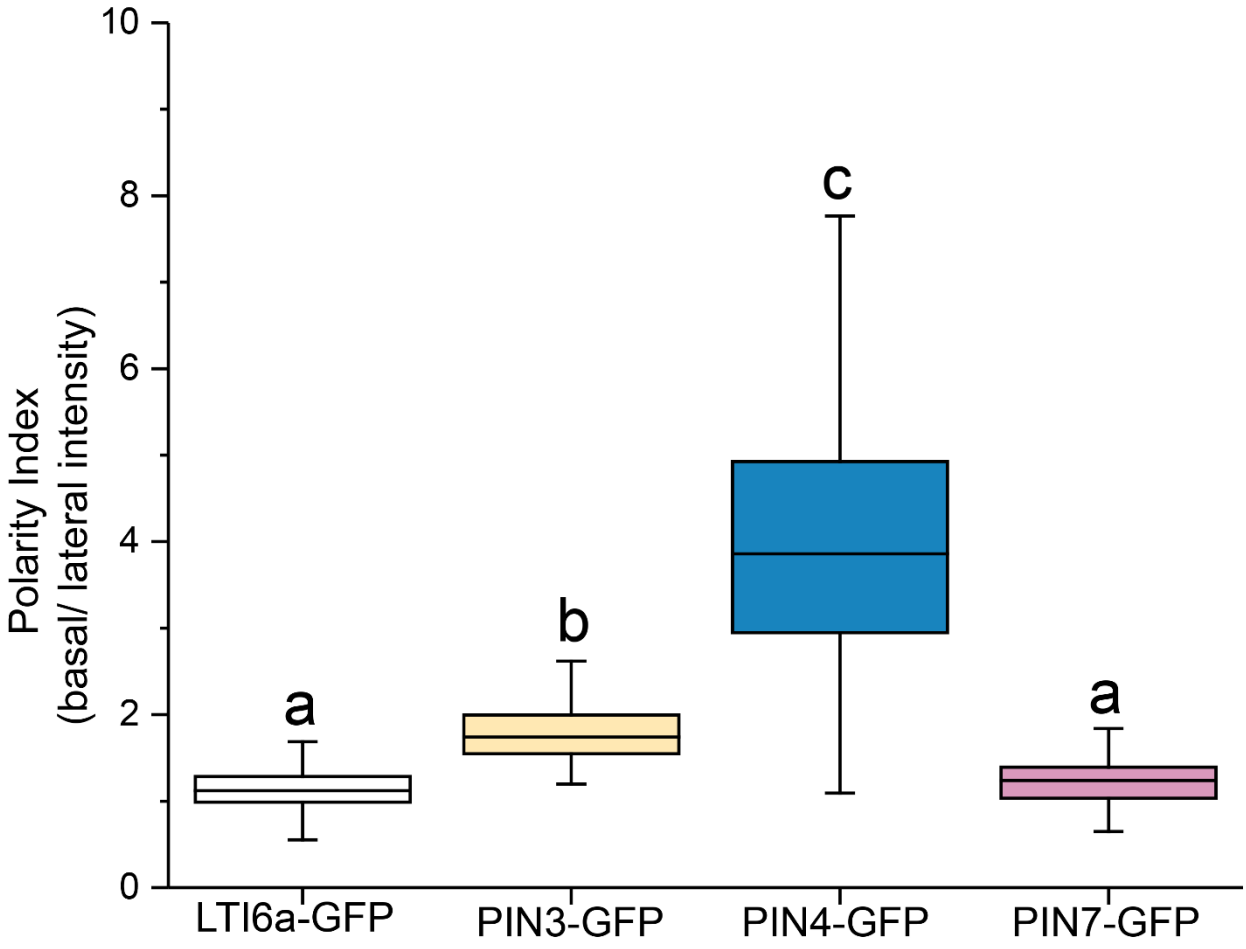

Fig. S5 Quantification of polarity index (basal/ lateral fluorescence intensity) of PIN3-GFP, PIN4-GFP, PIN7-GFP and LTI6a-GFP in hook epidermal cells. Polarity index was measured for at least 100 cells from 10 seedlings/ group. Polarities of PINs are compared with the nonpolar localization of LTI6a-GFP by one-way ANOVA with Tukey's post-hoc test. Groups with significant differences ($P < 0.05$) are indicated by different letters.

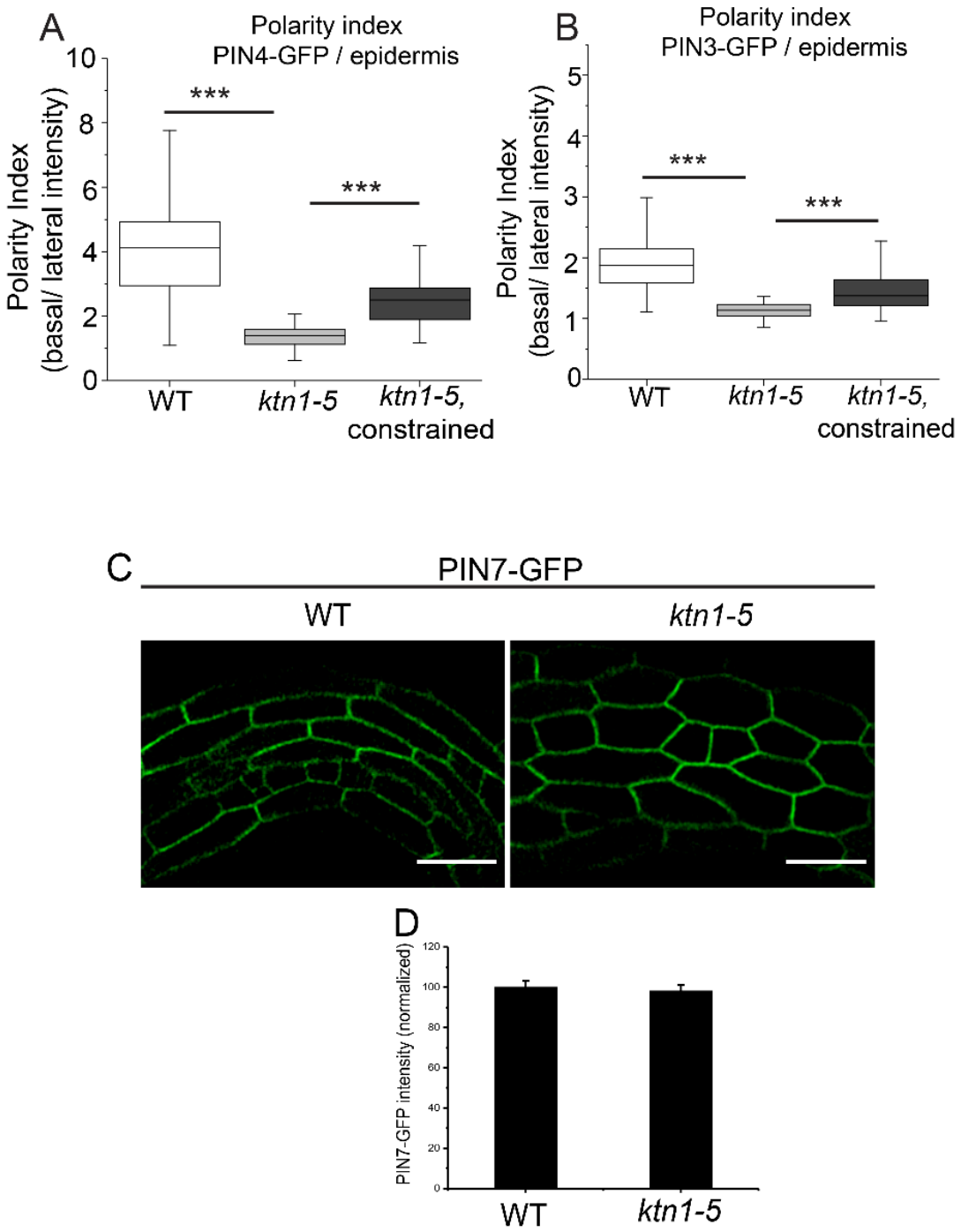

Fig. S6 Quantification of polarity index (basal/ lateral fluorescence intensity) of PIN4-GFP (A) and PIN3-GFP (B) in epidermal cells (related to Fig. 3A and 3B). Polarity index was measured for at least 100 cells from 10 seedlings/ group. Box plots show the first and third quartiles, split by the median; whiskers extend to minimum and maximum values. Asterisks (***) indicate $P < 0.0001$, ns = non-significant at $P \leq 0.05$ (Student's two tailed t-test). (C) Localization of PIN7-GFP in WT and *ktn1-5* hook region. (D) Quantification of PIN7-GFP intensities in WT and *ktn1-5* hook. At least 100 cells from 10 seedlings per group were measured. Bars represent normalized mean ± S.E.M, ns = non-significant at $P \leq 0.05$ (Student's two tailed t-test).

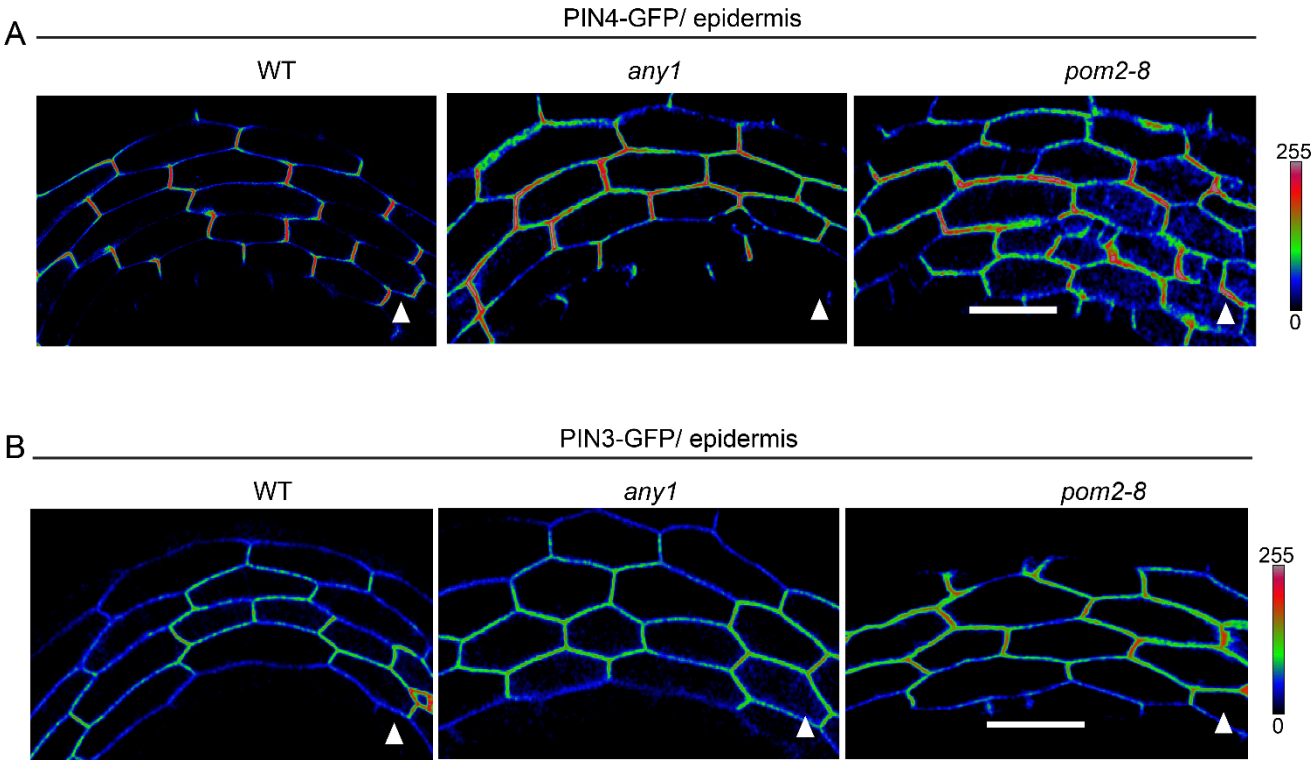

Fig. S7 Representative images of PIN4-GFP (A), PIN3-GFP (B) in epidermal cells of WT, *any1* and *pom2-8* apical hook. Triangles denote the end of the hypocotyl with the shoot apical meristem. Scale bar = 50 μm. Color bars in (A) and (B) represent 8-bit intensity range of 0-255.

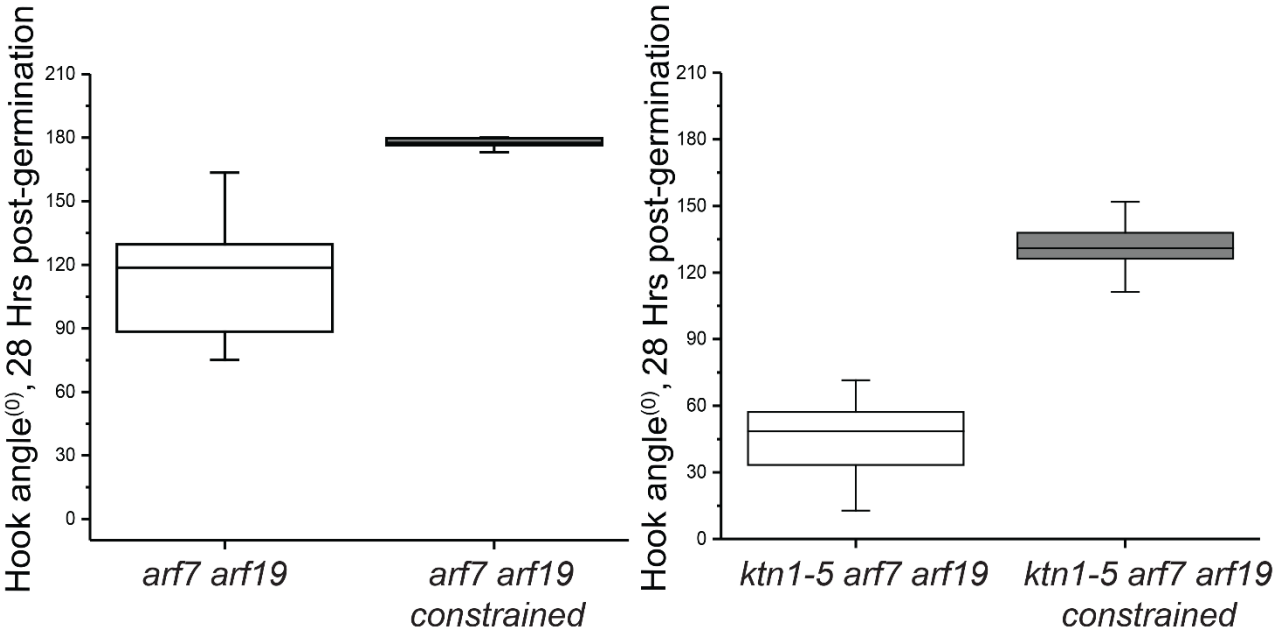

Fig. S8 Mechanically constrained hook formation is not dependent on ARF7 and ARF19. Quantification of apical-hook angles in *arf7 arf19* (A) and *ktn1-5 arf7 arf19* (B) seedlings. growing on the surface of MS agar or growing through the gel (constrained), 28 Hrs after germination, n = 16 seedlings/ group. Box plots showing the first and third quartiles, split by the median; whiskers extend to minimum and maximum values.